Fibration Symmetries and Cluster Synchronization in Multi-Body Systems

Margherita Bertè[1, *] and Tommaso Gili[1, †]

[1] *IMT School for Advanced Studies, P.zza San Francesco 19, 55100 Lucca (Italy).*

(Dated: October 14, 2025)

Based on recent advances in fibration symmetry theory, we investigate how structural symmetries influence synchronization in systems with higher-order interactions (HOI). Using bipartite graph representations, we identify a node partition in fibres, based on equivalent incidence relations in hypergraphs. We study how identical nodes with an isomorphic input set can synchronize due to structural properties under our specific model assumptions, examining the dynamical model of Kuramoto with higher-order interactions and frustration parameters. Recent works [1, 2] established for directed hypergraphs that balanced partitions characterize robust synchrony, invariant under all admissible dynamics, whereas our contribution isolates the case of Kuramoto dynamics and shows that synchrony under homogeneous initial conditions and natural frequencies necessarily coincides with the fibration partition. As a conclusion, let us examine situations that require adjustments to the hypergraph topology to handle redundancy or to align with a target cluster configuration, especially in the presence of noise or incomplete information. These considerations open up new questions for future investigations. Our methodology combines theoretical modeling and simulations with applications to real-world data topologies, highlighting how representational choices and local input equivalence influence synchronization behavior.

Keywords: fibration symmetries, higher-order interactions, cluster remote synchronization, Kuramoto model with frustration

I. INTRODUCTION

The study of symmetry in complex systems has been central to uncovering principles governing collective dynamics, particularly synchronization. Classical approaches, grounded in group theory and graph automorphisms, have revealed how structural features shape the evolution of connected systems. Yet in many biological and technological networks, global symmetries are rare. This has led to a shift toward local symmetry frameworks, utilizing groupoid theory rather than traditional group theory. Groupoids, introduced by Brandt in 1926, have since served various mathematical contexts [3], offering a generalized framework that extends and relaxes group properties. In our context, we focus on groupoids made by graph fibrations symmetries, which partition nodes based on equivalence in their input flows and have proven effective in identifying cluster synchronization patterns. Indeed, graph fibrations, a concept rooted in category theory [4], provide a useful framework to uncover synchronization patterns in complex networks and their relation with the topology [5–7].

While extensive research has focused on fibration symmetries in graphs, the growing interest in systems with higher-order interactions requires further development in this area. In such systems, interactions are not limited to pairs but involve groups of nodes, posing new challenges for understanding how structure governs dynamics. Refer to [8, 9] for reviews on complex systems with HOI. In this work, we use the terms *higher-order interactions* and *multi-body interactions* interchangeably, as they both refer to relations involving more than two nodes; no ambiguity arises regarding higher-order expansions. We position our work within this landscape by focusing on the generalization of fibration symmetries to HOI systems, relating to the recent contributions of Von der Gracht et al. [2], and guided by foundational insights from Boldi [10], Aguiar et al. [1], and Salova et al. [11] on bipartite representations. Notably, the comprehensive work [12] about fibrations symmetries dedicates a chapter to fibrations for higher-order interactions.

We also aim to prove how local structural equivalences can relate to partial synchronisation in a Kuramoto model, even between nodes that are not directly connected [13]. This emphasizes the relevance of remote synchronization phenomena, which can arise independently of global automorphism symmetries. To this end, we focus on a nonlinear dynamical model, which allows us to capture complex behaviors that more abstract linear approaches might miss, as highlighted in [2]. We focus on fibration symmetries, as they offer a principled way to partition nodes based on identical input structures. This choice differentiates our approach from other similar studies that refer in general to symmetries or equitable partitions, [1, 11]. Indeed, this notion, which corresponds to the coarsest equitable partition or minimal balanced coloring, is central to our analysis not only for its connection to dynamics but also

* margherita.berte@imtlucca.it
† tommaso.gili@imtlucca.it

because it captures intrinsic structural regularities that are relevant on their own. Building on the theoretical results of [1, 2] for directed hypergraphs, who proved that balanced partitions characterize robust synchrony invariant under all admissible dynamics, we restrict attention to the higher-order Kuramoto model with frustration, showing that clusters of synchrony coincide with the fibration partition under our model assumptions.

Recent studies on Kuramoto models with bi and triadic interactions highlight that the impact of higher-order interactions on total synchronization can nontrivially alter both the linear and basin stability of Kuramoto dynamics [14] and that depend on the chosen representation, enhancing or suppressing collective synchronization in hypergraphs versus simplicial complexes [15]. This point aligns with recent findings by Salova et al. [16], who emphasized the impact of representational choices on synchronization dynamics. We extend this perspective by showing that, beyond representation, the fibre structure itself shapes synchronization patterns, suggesting an interplay between network architecture and emergent behavior. Our analysis establishes that, starting from the agnostic case of identical oscillators with identical initial conditions, synchronous states not aligned with the fibration decomposition are instantaneously destabilized by mismatches in the input tree of the nodes. The invariant synchronized clusters correspond to the fibres. By integrating theoretical insights with empirical evidence, our research provides a conceptual framework and methodologies for examining HOI systems via fibration symmetries.

In the concluding section, we discuss the practical challenges encountered with hypergraph fibrations in symmetry-driven network modification [17–19]. First, we examine hypergraph sparsification methods that preserve fibre structures while removing redundant hyperedges to reduce computational complexity and improve interpretability. Second, we investigate topology modification techniques to reconstruct hypergraph structures when observed synchronization patterns suggest that the available topology may be incomplete or corrupted due to measurement limitations or data loss.

The structure of this work proceeds as follows. We first introduce notations and definitions to establish the concept of fibres for hypergraphs. Subsequently, we examine the phenomenon of partial synchronization in dynamical systems, specifically investigating the Kuramoto model with higher-order interactions and frustration parameters. In this context, we study local synchronization patterns while avoiding global synchronization regimes, and we analyze the relationship between fibres and the evolution of synchronous groups of nodes, showing that these two partitions coincide under specific model assumptions. In the concluding section, we address the challenge of altering hypergraph topology to restore or impose symmetries, including sparsification techniques that maintain fibre structures and reconstruction approaches for matching target fibre partitions. Throughout the paper, we provide visualizations and examples to illustrate key concepts, maintaining an operative perspective through algorithmic implementations and references to real-world network topologies.

Related works

Graph fibrations and symmetry-based methods have been widely explored across different domains to understand synchronization and collective dynamics, from distributed computing [5], gene regulatory systems [20], to the neuronal network [21]. Recent advancements in network theory have shed light on the deep connection between network structure and function, particularly through the lens of graph fibrations and symmetry groups [5–7, 22].

In the context of biological networks, Morone et al. [21] applied symmetry group factorization to the neural connectome of *Caenorhabditis elegans*, showing a hierarchical structure that matches broad functional categories. Further, Leifer et al. [20] applied fibration symmetries to predict synchronized gene coexpression patterns in bacterial gene regulatory networks. Their findings suggest that network structure alone can provide valuable insights into gene synchronization, potentially reflecting evolutionary pressures that have shaped gene input functions to realize coexpression. The application of these theoretical frameworks to human brain networks is beginning to yield insights into cognitive function. Makse et al. [23] applied fibration symmetry analysis to brain networks involved in language processing, revealing how symmetry breaking supports functional transitions between resting state and language engagement. This work suggests that local network symmetry in the brain may play a crucial role in determining coherent function, offering a new perspective on the structure-function relationship in neuroscience.

In all cases where global symmetries do not apply, as in the biological realm, the shift of focus from global to local patterns and their impact on the entire system has gained more attention. With this perspective, cluster synchronization refers to the phenomenon where subsets of nodes in a network synchronize their dynamics while remaining out of sync with nodes in other clusters. This behavior is often associated with structural symmetries or equitable partitions in the network, which constrain the dynamical evolution and lead to partial synchronization patterns. Different works focus on the concept of cluster (or partial) synchronization. On the one hand, providing computational perspectives through algorithms to partition the nodes [24] or to optimize the analysis of stability for local dynamical patterns [25]. On the other hand, providing a case study or a unified framework and theory related to dynamical processes and node partition [11, 26, 27].

The Kuramoto model describes coupled phase oscillators and typically leads to global synchronization under strong coupling when natural frequencies are identical. To capture more complex phenomena, such as partial or inhibited synchronization, researchers have extended the model by introducing phase-lag (frustration) terms. Nicosia et al. [13] linked these frustrated dynamics to remote synchronization mediated by network symmetries, a relationship further explored in the comprehensive overview on cluster synchronization [28]. Kirkland et al. [29] introduced α-Kuramoto partitions to study synchronization patterns constrained by a phase lag, while Brede [30] explored heterogeneous phase shifts via local frustration parameters.

Beyond pairwise interactions, higher-order interactions generalize the notion of connectivity to groups of nodes, posing additional challenges for analyzing partial synchronization. Recent studies on hypergraphs or simplicial complexes often rely also on equitable partitions to understand these patterns [1, 11]. Multi-body generalizations of the Kuramoto model, incorporating frustration or phase-lag parameters, have been proposed to capture more complex dynamical behaviors. However, existing generalizations have primarily focused on all-to-all configurations. Notable contributions include Dutta et al.'s asymmetric Kuramoto model for hypergraphs [31], which generalizes frustration to higher-order interactions, Moyal et al.'s work specifically addressing frustration in hypergraphs limited to three-body interactions [32], and León et al. [33], who showed that higher-order interactions with nonzero phase-lag in globally coupled ensembles can produce anomalous transitions to synchrony.

In parallel, for multi-body interactions, the study of local symmetries has provided a structural perspective on cluster synchronization [1, 2]. In particular, Von der Gracht et al. formally extended the notion of fibrations to systems with higher-order interactions and demonstrated that balanced partitions induced by fibrations identify robust synchrony spaces for all admissible dynamics. Our contribution lies in connecting the structural framework of fibrations with the dynamical insights of the Kuramoto model for multi-body interactions. First, we adopt a structural perspective, analyzing fibration symmetries in hypergraphs and examining how multi-body representations affects node clusters and partial synchronization patterns. We propose a different representation of HOI using bipartite graphs, following the insights in [1, 10]. This approach enables leveraging the algorithms of graph theory to compute fibres. We then focus on a principled Kuramoto model with two- and three-body interactions [33] and show that, under specific assumptions, the resulting synchronization clusters coincide with the fibration partition.

II. GRAPH FIBRATION SYMMETRIES

This section introduces the formal mathematical definitions of graph fibrations. Further, by fixing the notation and presenting common basic definitions, the aim is to provide a unified framework to facilitate the interpretation of the concepts discussed throughout this work and as a reference point for extending fibration symmetries to complex systems with higher-order interactions.

Definition II.1 (Directed graph)**.** A directed graph G is a tuple $G = (N, E, s, t)$ where N is the set of nodes and $E \subseteq N \times N$ is the set of edges. The source and target maps, respectively $s, t : E \to N$, associate each edge with its tail or head, namely the first or second nodes in the ordered pair of nodes constituting the edge.

Definition II.2 (Undirected graph)**.** An undirected graph $G = (N, E, s, t)$ is a directed graph such that $\forall e \in E$, $e = (s(e), t(e)) \Rightarrow \exists f \in E$ s.t. $f = (t(e), s(e))$.

Remark II.3. An undirected graph can be characterized by specifying only the set of nodes and edges. Hence, we will omit the source and target maps.

We now proceed to define fibration symmetries for directed graphs, adopting the notation by Boldi et al. [5] who first organized and presented systematically the fibration symmetries theory for graphs.

Definition II.4. Let $G = (N_G, E_G, s_G, t_G), B = (N_B, E_B, s_B, t_B)$ be directed graphs. A **graph homomorphism** $\xi : G \to B$ is given by a pair of functions $\xi_N : N_G \to N_B$ and $\xi_E : E_G \to E_B$ commuting with the source and target maps.

A **fibration** between G and B is a homomorphism $\varphi : G \to B$ such that $\forall a \in E_B, \forall x \in N_G$ satisfying $\varphi(x) = t_B(a)$ there is a unique arc $\tilde{a}^x \in E_G$ such that $\varphi(\tilde{a}^x) = a$ and $t_G(\tilde{a}^x) = x$. In literature, we refer to G as the total graph and to B as the base graph. This property is called the lifting property.

A **fibration symmetry** is a surjective minimal fibration.

Nodes mapped in the same node in the base graph B are a **fibre**. A trivial fibre is a singleton.

Remark II.5. Theorem II.4 can be extended to undirected graphs by treating them as bidirected graphs, meaning that each undirected edge is regarded as two directed edges that connect the two possible configurations of source and target vertices.

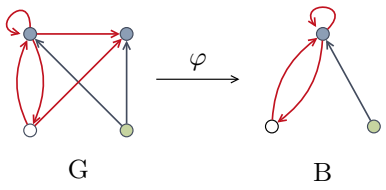

Figure 1: Example of graph fibration $\varphi : G \to B$. Nodes with the same color belong to the same fibre in the total graph G and are mapped by φ to the unique node with the same color in the base graph B, which is the quotient graph.

Makse et al. [12] provide a detailed discussion of the different notions of graph quotients that arise when one takes a node partition as an equivalence relation. The definition is subtle, since different conventions lead to different objects. In our setting, we require the quotient to coincide with the base graph in the sense of fibration symmetry. In particular, the construction must guarantee the lifting property.

Definition II.6 (Quotient graph)**.** Let $G = (N, E)$ be a directed graph and let $\sim$ be the equivalence relation on N induced by a fibration symmetry, i.e., $u \sim v$ whenever u and v belong to the same fibre. For $v \in N$, denote by $[v]$ the fibre containing v.

The quotient graph $G/\sim := (\bar{N}, \bar{E})$ is defined as follows:

- The node set is $\bar{N} = \{[v] \mid v \in N\}$.
- For an ordered pair of fibres $[u], [v] \in \bar{N}$, the number of directed edges between them in $\bar{E}$ equals the number of edges in G between a vertex of $[u]$ and a vertex of $[v]$.
- If u and v lie in the same fibre, loops in $\bar{E}$ record the edges of G internal to that fibre.

Thus, the quotient graph is obtained by collapsing each fibre to a single node while preserving the connectivity pattern between fibres. In Figure 1, we depict a representation where nodes in the same fibre (with the same color) are collapsed into a unique node in the quotient graph on the right (also named base graph). We can observe that the fibration symmetry φ maps each node to a quotient node whose incoming edges originate from nodes of the same fibres as in the total graph.

III. HIGHER-ORDER INTERACTIONS

This section sets the notations needed to model higher-order interactions in complex systems. We recall the definitions of hypergraphs and their associated bipartite representations. We then emphasize how the incidence bipartite graph provides a natural framework for identifying fibres in multi-body interactions. Finally, we introduce the notions of fibres and fibration symmetries in the context of hypergraphs.

Definition III.1 (Directed hypergraph)**.** A directed hypergraph $H = (N, E)$ consists of a node set N and a a set of directed hyperedges E. A directed hyperedge $e \in E$ is a pair $(T(e), H(e))$, where the tail $T(e)$ is a non-empty multiset of elements of N and the head $H(e)$ is a non-empty subset of N.

Remark III.2. In our setting, we do not require an order among the nodes in the tail or or head of each hyperedge, differently from [2].

As a particular case of directed hypergraphs, we can consider undirected hypergraphs (hereafter referred to as hypergraphs). They will be the focus of our work.

Definition III.3 (Hypergraph)**.** An undirected hypergraph $H = (N, E)$ consists of a node set N and a hyperedge set E, where each hyperedge is a non-empty multiset of nodes from N. The cardinality of a hyperedge is called its order. The rank $rk(H)$ of a hypergraph is the maximum of the orders of its hyperedges, $rk(H) = \max_{e \in E} |e|$.

Remark III.4. Because hyperedges are multisets, a node may appear more than once within the same hyperedge. While this is not the standard convention in hypergraph theory, it is a natural choice when working with quotient constructions, and it has already been adopted in related contexts (e.g. [1, 2]). This convention will be important here to guarantee that the quotient of a hypergraph remains a hypergraph under the current definition (refer to the hypergraph on the right in Figure 3).

Remark III.5. An undirected hypergraph can be considered as a directed hypergraph with all possible combinations of source and target sets in each hyperedge, as nicely depicted in Figure 1 of [34].

Remark III.6. Observe that if $rk(H) = 2$, then H is an undirected graph.

Definition III.7 (Bipartite graph)**.** A bipartite graph is a graph $G = (N_1 \sqcup N_2, E)$ where the nodes can be partitioned into two disjoint subsets (named layers) such that $E \subseteq N_1 \times N_2 \vee E \subseteq N_2 \times N_1$. It means that the edges cannot contain nodes belonging to the same layer.

Incidence graph representation A hypergraph $H = (N, E)$ can be represented via its incidence bipartite graph $B_H = (N \sqcup E, F)$, where $F = \{(n, e) \in N \times E \,|\, n \in e\}$, also called factor graph [12]. In [10], the author proves a categorical equivalence between directed hypergraphs and bipartite RB-graphs. With the same perspective, in Section A we extend the demonstration and propose the categorical equivalence of the undirected hypergraphs and bidirectional bipartite graphs. This relationship is naturally intuitive, as the unique incidence matrix (apart from the order) of a hypergraph coincides with the unique bi-adjacency matrix of the bipartite graph having as nodes in the first layer the hypergraph nodes and as nodes in the second layer the hyperedges. Thus, a hypergraph can be handled by its incidence bipartite representation, and algorithms designed to partition graph nodes with the same input trees can be applied to hypergraph nodes by regarding them as belonging to an inhomogeneous directed graph.

Remark III.8. The bipartite graph must not contain any isolated node since disconnected nodes in the second layer would represent empty hyperedges, which fall outside the formal definition of a hypergraph.

IV. FIBRATION SYMMETRIES FOR HYPERGRAPHS

By representing the hypergraph as its incidence bipartite graph, we can treat it as an inhomogeneous graph and thus apply fibre-computing algorithms. In this perspective, nodes corresponding to original vertices and nodes corresponding to hyperedges are explicitly distinguished from the outset by assigning them different initial types (or colors). The algorithm then partitions both sets into fibres, producing a coloring of the original nodes as well as of the hyperedges (see Figure 2). The fibres in a hypergraph H are defined as the nodes that belong to identical fibres in the associated incidence bipartite graph B_H when B_H is treated as an inhomogeneous graph. Fibration symmetries for HOI are fibrations symmetries for the inhomogeneous graph representation of the incidence bipartite graph of the hypergraph, preserving the colors of the original nodes and hyperedges.

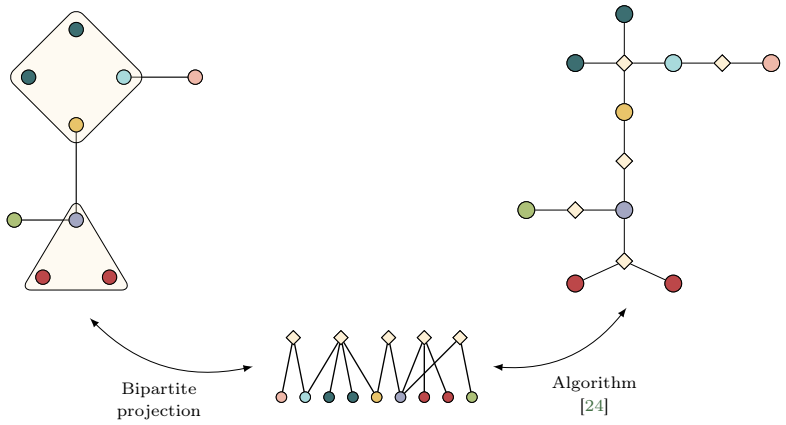

Figure 2: Starting from an undirected hypergraph, we can associate its incidence bipartite projection. Considering it as an inhomogeneous graph, we can apply standard graph algorithms, as the version of [24] revised by [35], to obtain the hypergraph node partition, here depicted with different colors.

For hypergraphs, the quotient construction is performed on the incidence bipartite graph, and the resulting quotient can then be translated back into the hypergraph setting. A key point is that preserving multi-body interactions may require allowing repeated occurrences of quotient nodes within the same hyperedge. Figure 3 illustrates a fibration symmetry on a hypergraph. Nodes on the left are mapped to nodes of the same shape and color on the right. In the quotient on the right, some nodes appear multiple times in a single hyperedge, highlighting the role of multisets in the definition of a hypergraph. It is also worth noting that, as for quotient in graphs, even if the original hypergraph is undirected, its quotient need not be. Indeed, when two distinct nodes of the same fibre are connected to a common

node in the original hypergraph, collapsing them in the quotient may introduce a non-reciprocated edge, thereby breaking undirectedness.

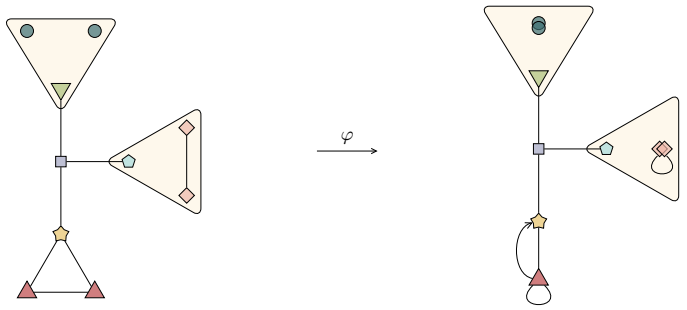

Figure 3: Hypergraph quotient via fibration symmetry. The left hypergraph shows the original structure where nodes with identical shapes and colors represent distinct vertices belonging to the same fibre under the fibration map φ (i.e., nodes receiving equivalent input information). The right side depicts the quotient hypergraph, where nodes with matching shapes and colors represent a single supernode corresponding to an entire fibre. In the quotient representation, slightly overlapping identical nodes within hyperedges indicate multiple instances of the same supernode participating in that hyperedge, preserving the structural information while reducing redundancy through the fibration symmetry φ. Edges without arrows are undirected (equivalent to having arrows in both directions).

Remark IV.1. Observe that different types of node partitioning can emerge depending on whether we analyze a hypergraph, its binary graph projection, or its multigraph projection. Each representation captures different structural features of the original hypergraph. The binary graph projection simplifies the hypergraph by representing only the existence of pairwise interactions, discarding information about the number or order of interactions. As a result, it overlooks distinctions between higher-order relationships and repeated interactions, leading to a fibre structure that lacks key information. In contrast, the multigraph projection preserves the multiplicity of interactions between pairs of nodes, capturing how frequently node pairs co-occur in hyperedges. However, it still treats all interactions as equivalent, regardless of their order, thus failing to distinguish the structural role of higher-order interactions.

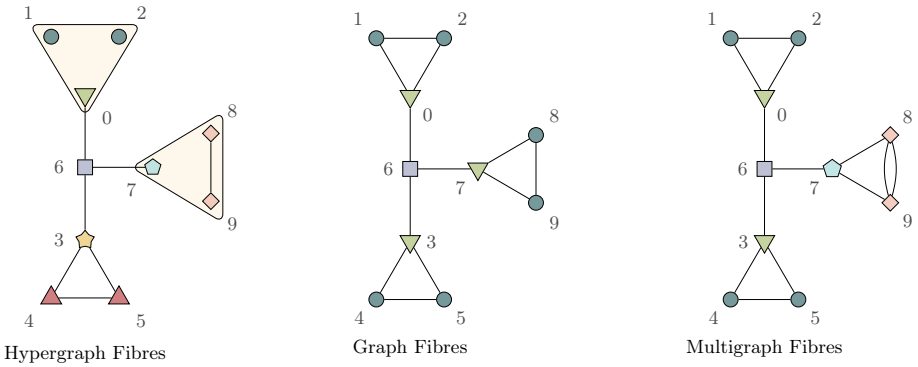

Figure 4: Example of fibres for a hypergraph, its projection to a simple graph, and its projections to a graph with multiple edges. In each representation, nodes belonging to the same fibres are pictured with the same color and icon.

This behavior is illustrated with an example in Figure 4. The left panel shows a hypergraph, where nodes are grouped into fibres based on their participation in higher-order hyperedges (represented by shaded regions). In the middle panel, the binary graph projection loses both the frequency and the order of these interactions, leading to a different and less informative fibre structure. The right panel, representing the multigraph projection, captures repeated pairwise connections but still ignores the order of the original hyperedges, resulting in a distinct partitioning.

A. Algorithm

In Section III, we discussed how, thanks to the equivalence of a hypergraph and its bipartite projection, we can utilize established algorithms, such as those presented in [24]. In this section, we report an algorithm to obtain the partition of the nodes of an input hypergraph according to the fibres. The following Algorithm 1 proceeds by projecting the hypergraph into its bipartite representation and then applying an iterative color refinement scheme. The notation and the steps follow the algorithm presented in [35]. Hence, the complexity to assign colors to nodes and hyperedges of a hypergraph $H = (N, E)$ scales as $O(|F|\, log(|N|+|E|))$, where F is the set of edges in the bipartite representation of H.

Algorithm 1: Finding fibres for a hypergraph via its bipartite graph projection .

Input: Hypergraph $H = (N, E)$, where N are the nodes and E are the hyperedges.
Output: $\{c_i\}_{i\in N}$, where c_i is the color of node i in N. $\{c_j\}_{j\in E}$, where c_j is the color of hyperedge j in E.
Step 1: Transform the hypergraph into its bipartite graph projection.
$G = (N \sqcup E, F)$ be the bipartite graph, where:

- Nodes of G consist of two disjoint sets: N (nodes of the hypergraph) and E (hyperedges of the hypergraph).
- Edges F connect nodes in N to the hyperedges in E they belong to.

Step 2: Assign starting colors.
foreach *node* $v \in N \sqcup E$ **do**
  if $v \in N$ *(nodes of the first layer)* **then**
    Assign initial color $c_v = 0$.
  else if $v \in E$ *(nodes of the second layer)* **then**
    Assign initial color $c_v = 1$.
  end
end
Step 3: Apply the iterative coloring algorithm.
$j \leftarrow 0$
$R_0 \leftarrow 1$
repeat
  for $i = 1$ **to** $|N \sqcup E|$, $k = 0, \ldots, R_j$ **do**
    $I_i^k \leftarrow$ number of nodes of color k in the input set of i
  end
  $I \leftarrow$ set of all unique $I_i := \{I_i^k\}_k$ (an ordered list of I_i^k)
  for $i = 1$ **to** $|N|$ **do**
    $c_i \leftarrow$ index of I_i in I (e.g., if two nodes have the same I_i and $I_j \rightarrow c_i = c_j$)
  end
  $j \leftarrow j + 1$
  $R_j \leftarrow |I|$
until $R_j \neq R_{j-1}$;
Step 4: Extract final colors for nodes of the first layer and for nodes of the second layer.
return $\{c_i \mid i \in N\}$ *(colors of the hypergraph nodes),* $\{c_j \mid j \in E\}$ *(colors of the hyperedges).*

B. Fibration symmetries for real-world datasets with HOI

To illustrate the relevance of fibration symmetries beyond theoretical models, we analyze several real-world systems featuring higher-order interactions. We computed the nodes partition via fibration symmetry for some datasets with higher-order interactions provided by XGI dataset [36]. In addition, we calculated the fibres for an emblematic example of higher-order interactions in real-world situations: collaborations among researchers for publishing a paper in a conference. We considered the MAG-10 dataset[1] [37, 38], a subset of the Microsoft Academic Graph in which the nodes are the authors (labelled with a code), the hyperedges correspond to a publication by those authors, and the hyperedges are categorised according to one of the 10 computer science conferences, the most common conference in which they published. In particular, we considered the *International Conference on Machine Learning* (ICML),

[1] preprocessed in https://github.com/TheoryInPractice/overlapping-ecc/tree/master/data/MAG-10

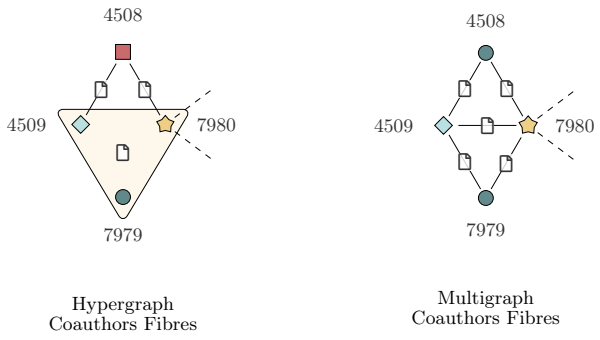

Figure 5: Example of different fibres between the hypergraph representation and its multigraph projection in a real-world case for collaboration on publications for the ICML conference (MAG-10 dataset filtered for ICML conference). Nodes represent authors, and paper collaborations are depicted with a hyperedge among the authors, stressed with a paper icon. Nodes painted with the same color and mark belong to the same fibre. For the sake of the example, in this image, we represent only the papers related to authors labeled with codes 7979 and 4508. Nodes 4509 and 7980 are in different fibres in both cases as they are related (illustrated with dashed lines) to different other nodes not present in the picture.

filtering by code 3, the *International World Wide Web Conference* (WWW), filtering by code 2, and the *International Conference on Computer Vision* (ICCV) with code 8. In this dataset, articles with more than 25 authors are omitted.

Dataset	$\|N\|$	$\|E\|$	$\|N\|/\|C\|$	# Non-trivial fibres
diseasome	516	314	1.46	94
disgenenet	12368	1672	1.39	629
hospital-lyon	75	1824	1.00	0
house-committees	1290	335	1.07	51
hypertext-conference	113	2434	1.00	0
invs13	92	787	1.00	0
MAG-10 (ICML)	9981	4803	2.32	1354
MAG-10 (WWW)	12889	5468	2.42	1829
MAG-10 (ICCV)	11693	5367	2.30	1683
malawi-village	84	431	1.01	1
ndc-classes	628	796	1.51	165
ndc-substances	3414	6471	1.16	248
plant-pollinator-mpl-015	130	401	1.02	2
plant-pollinator-mpl-016	26	73	1.04	1
plant-pollinator-mpl-049	37	91	1.00	0
plant-pollinator-mpl-062	456	866	1.00	0
science-gallery	410	3350	1.00	1

Table I: Table reporting for each dataset, the number of nodes $|N|$, the number of edges $|E|$ excluding singletons. Considering $|C|$ as the number of fibres partitioning the nodes via higher-order symmetry fibrations, we report the average number of nodes in each fibre $|N|/|C|$ and, in the last column, the number of nontrivial fibres, all the fibres formed by more than one node.

As observed in Theorem IV.1, for the MAG-10 dataset related to the ICML conference, representing paper collaborations through a hypergraph rather than a multigraph alters the fibres. The case depicted in Figure 5 illustrates how, in the multi-edge projection, the two authors with codes 7979 and 4508 are placed in the same fibre, despite having collaborated in different ways with the same authors (with codes 4509, 7980). Indeed, while the author 7979 collaborated on one paper with the other two authors 4509, 7980 together, the author 4508 produced two papers in two different collaborations with each of the individual authors. The graph representation with multiple edges flattens this case by not recognizing the different types of collaboration by bringing them together. An analogue mismatch occurs for the dataset corresponding to the publication in the International World Wide Web Conference. Specifically, at WWW, the author identified as 21331 co-authored two separate papers with authors 21332 and 22750, while the author with code 32176 collaborated with both on a single paper. In the multigraph representation, a fibre includes authors 32176 and 21331, failing to differentiate their distinct publishing contributions. The same situation occurs

for the two pairs of authors with code 18628, 51267 and 2149, 37684 related to ICCV.

V. CLUSTER SYNCHRONIZATION

Having established the structural foundations through definitions and illustrative examples of fibrations for higher-order interactions, we now turn to the dynamical aspects of the system. To ensure compatibility between the dynamics and the underlying hypergraph structure, we consider admissible ODE systems [1, 2], where the evolution of each node depends only on the structure-prescribed interactions. The higher-order Kuramoto model with frustration (Kuramoto-Sakaguchi) falls within this class, as its dynamics respect the hypergraph topology and involve only interactions explicitly defined by the system's combinatorial structure. In this section, we introduce the dynamical model and examine how the underlying structural features influence its behavior. We aim to connect the structural characterization of robust synchrony due to Von der Gracht et al. and Aguiar et al. with the behavior of the higher-order Kuramoto dynamics, showing in particular that synchrony in this model with homogeneous initial conditions and natural frequencies is constrained to the fibration partition.

A. Higher-order Kuramoto model with phase-lag parameters

We study synchronization dynamics in oscillator populations using a Kuramoto model with both pairwise and three-body interactions. Although our framework refers broadly to higher-order interactions, we focus on two- and three-body terms as the minimal setting that captures collective behaviors beyond standard pairwise coupling. Our primary interest lies in cluster and remote synchronization, where phase alignment of identical oscillators occurs only within specific groups of nodes, rather than across the entire network. The inclusion of three-body interactions follows the principled derivation of León et al. [33], who used phase reduction techniques to show that such interactions naturally arise in the form $\sin\left(\theta_\gamma + \theta_\delta - 2\theta_a - \alpha\right)$ for an oscillator a. While León et al.'s formulation assumes all-to-all coupling, we generalize it to arbitrary network topologies, in line with Muolo et al. [39]. Crucially, we retain the phase-lag parameter, which prevents trivial global synchronization and enables the network to exhibit nontrivial collective states, even with identical oscillators starting with identical initial conditions.

Model Consider a hypergraph $H = (N, E)$, with rank $rk(H) \leq 3$. Define the incidence matrix of order m with $m \in \{2, 3\}$ as the matrix $I^{(m)}$ with as many rows as the cardinality of N and as many columns as the cardinality of $\mathcal{E}^{(m)} = \left\{e \in E \mid |e| = m\right\}$, that is the set of hyperedges of order m. Then $\forall i \in N, e \in E$:

$$[I^{(m)}]_{i,e} = \begin{cases} 1 & \text{if } i \in e \\ 0 & \text{otherwise} \end{cases}$$

The evolution of each node $i \in N$ can be expressed as follows:

$$\dot{\theta}_i = \omega_i + \sum_{m=2}^{3} \sigma_m \sum_{e \in \mathcal{E}^{(m)}} [I^{(m)}]_{i,e} \sin\Big(\sum_{j \in e \setminus \{i\}} \theta_j - (m-1)\theta_i - \alpha^{(m)} \Big), \tag{1}$$

where σ_m is the strength of the mth order coupling and ω_i is the natural frequency of the oscillator associated with the node. Angles $\alpha^{(m)} \in (0, \pi/2)$ are the phase frustration parameters for each order m. The frustration parameters prevent the system from achieving global synchronization (unless all nodes belong to a single trivial cluster), instead allowing the emergence of partial or cluster synchronization patterns. To isolate the role of the network structure and frustration in shaping these patterns, we will assign identical initial conditions and natural frequencies to all nodes. This choice reflects an anonymity condition in the sense of [12], ensuring that any observed symmetry breaking arises purely from the dynamics and topology, rather than from imposed heterogeneity.

Remark V.1. We observe that the coupling function of the Kuramoto model for identical oscillators with phase-lags $\alpha^{(m)} = 0$ for all m is non-invasive (i.e., evaluated in $\theta_i = \theta^*$ for all i is identically 0). Hence, a solution exists for global system synchronization. By inserting non-zero $\alpha^{(m)}$ instead, we avoid this case.

Synchronization measures A common way to measure coherence among a subset of nodes evolving according to a Kuramoto model is to compute the Kuramoto order parameters. We will compare global and cluster order parameters to analyze their evolution in time.

Definition V.2 (Kuramoto Order parameters)**.** The global Kuramoto order parameter is defined as

$$R(t) = \left| \frac{1}{|N|} \sum_{j \in N} e^{i\theta_j(t)} \right|$$

where $R(t) \in [0, 1]$ quantifies the overall phase coherence of the system. Given a cluster $C_\alpha \subseteq N$, the local order parameter is

$$R_\alpha(t) = \left| \frac{1}{|C_\alpha|} \sum_{j \in C_\alpha} e^{i\theta_j(t)} \right|$$

where $R_\alpha(t) \in [0, 1]$ measures the synchronization within cluster C_α.

The Kuramoto order parameter is a measure of phase coherence among a group of oscillators. It takes values between 0 and 1, where 1 indicates perfect synchronization, all nodes are in phase, while values closer to 0 reflect increasing incoherence.

All simulations carried out throughout the paper, unless otherwise stated, solve the Cauchy problem by computing trajectories using the Runge-Kutta explicit method of order 5 (`dopri5`) from the Python library SciPy with step size 0.1, and synthetic hypergraphs are generated using `random_hypergraph` from the `hypergraphx.generation.random` module from the Python library Hypergraphx by specifying the number of nodes and hyperedges of orders 2 and 3, then extracting the largest connected component.

Figures 6 to 8 present the temporal evolution of global and local order parameters for fibre configurations across three hypergraph architectures: synthetic networks, plant-pollinator systems, and the diseasome. In all the images, we can see that at $t = 0$ all the parameters are 1, as the initial conditions are set equal for all nodes. During the evolution, local order parameters for fibre clusters remain constant at unity across all hypergraph types, while global order parameters exhibit deviations from unity. This divergence indicates that global coherence breaks down despite the preservation of local cluster organization, indicating the influence of network topology on these dynamics.

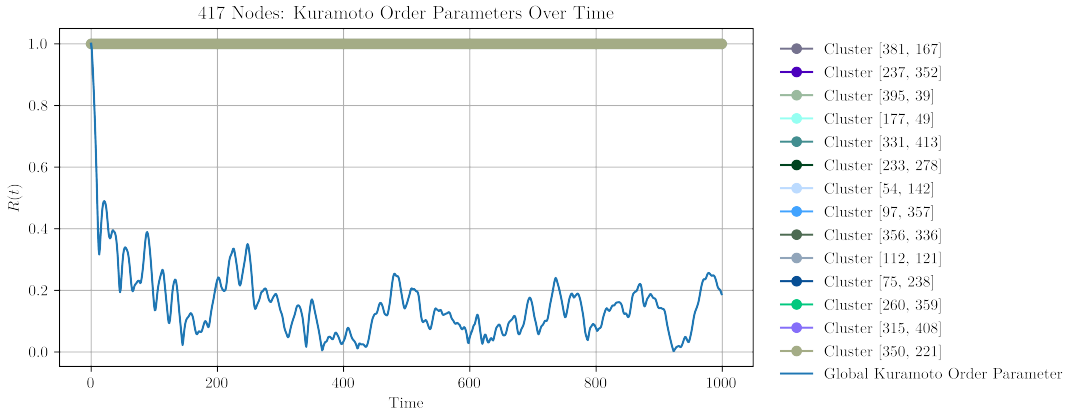

Figure 6: The Kuramoto order parameters R for different fibres and for the whole hypergraph for a higher-order Kuramoto model with frustration (Equation (1) with $|N| = 417$, $\alpha = \pi/6$ and $(\sigma_2, \sigma_3) = (0.2, 0.6)$). When R is closer to 1, the phases of all nodes are more synchronized. The local order parameters for all fibres overlap and are identically 1. The blue thin line is the global order parameter.

B. Fibration and Kuramoto synchrony partitions in the Kuramoto model

Let's analyse the relations between the nodes' partition of a hypergraph in fibres and a Kuramoto synchrony partition starting from identical initial conditions and natural frequencies for all nodes. We first recall that the implication *fibration partition* $\Rightarrow$ *Kuramoto synchrony partition* (Theorem V.4) follows directly from the general theory [2] as the vector field associated with our model is admissible. We include a proof in the specific Kuramoto setting for completeness. The second implication proved in Theorem V.7 addresses the converse direction: in our

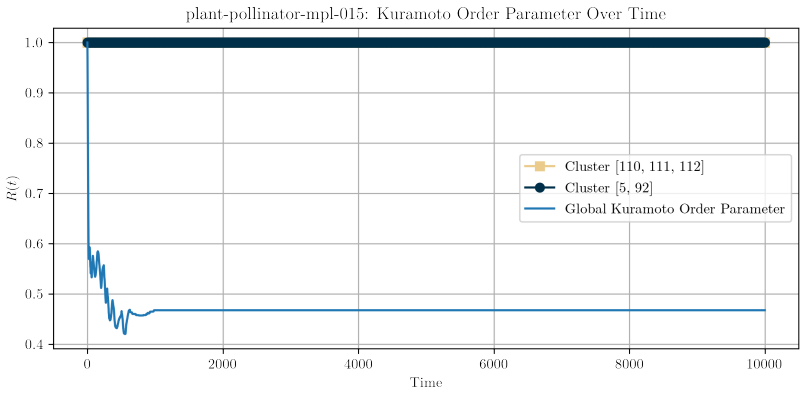

Figure 7: The Kuramoto order parameters R for the nontrivial fibre and for the whole hypergraph with a higher-order Kuramoto model with frustration (Equation (2), with $\alpha = \pi/6$). The topology is from a plant-pollinator real dataset. When R is closer to 1, the phases of all nodes are more synchronized.

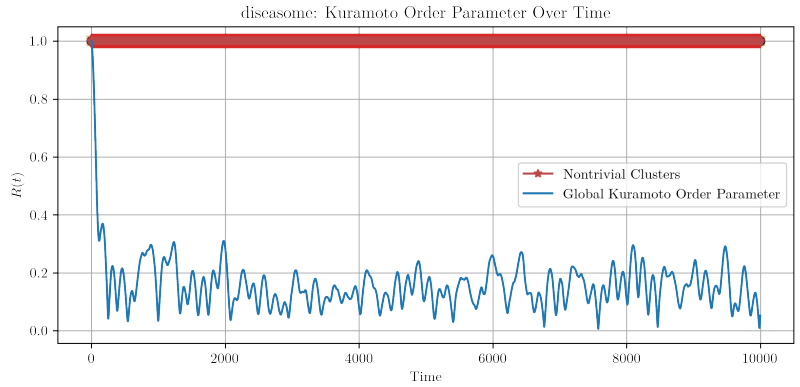

Figure 8: The Kuramoto order parameters R for the nontrivial fibre and for the whole hypergraph with a higher-order Kuramoto model with frustration (Equation (2), with $\alpha = \pi/6$). The topology is from the largest connected component without duplicate edges of the *diseasome* dataset (95 nontrivial clusters) [40]. In this dataset, a disease is a node, and a gene is a hyperedge. When R is closer to 1, the phases of all nodes are more synchronized. In red, the overlapped fibre order parameters are identically equal to 1 for all 95 non-trivial fibres.

restricted Kuramoto framework with homogeneous initial conditions and natural frequencies, any Kuramoto synchrony partition must coincide with the fibration partition, except on a parameter set of measure zero. To introduce the notion of a subspace of the hypernetwork's total phase space characterized by the equality of node phases, we define a Kuramoto synchrony partition of the nodes according to their trajectories. We generalize the definition of α-Kuramoto partition [29] to emphasize the dynamical nature of these partitions in the context of the Kuramoto model with frustration.

Definition V.3 (Kuramoto synchrony partition)**.** Given an undirected hypergraph $H = (N, E)$ with rank $rk(H) \leq 3$, take a set of 2 parameters $\{\alpha^{(m)}\}_{m\in\{2,3\}}$ with every $\alpha^{(m)} \in (0, \pi/2)$. Consider the trajectories θ_i for the nodes resulting from the Equation (1) with parameters $\{\alpha^{(m)}\}_m$, identical natural frequencies $\omega_i = \omega$ and initial conditions $\theta_i(0) = \theta_i^0, \quad i \in N$ for all nodes. We call Kuramoto synchrony partition the node partition $N = S_1 \sqcup \cdots \sqcup S_h$ such that:

- $i, j \in S_a$ if $\theta_i(t) = \theta_j(t)\ \forall t \geq 0$.
- if $i \in S_a$ and $\ell \in S_b$ with $a \neq b$, then there exists some $t \geq 0$ such that $\theta_i(t) \neq \theta_\ell(t)$.

In a nutshell, nodes with the same trajectories for all the process are in the same cluster, while nodes with different trajectories must be in different clusters. Observe that belonging to the same cluster results in the same trajectory for all t, which we can indicate with the cluster index $\theta_i(t) = \theta_a(t)$ for all nodes i in cluster S_a. We can reduce the

number of frustration parameters to just one α angle belonging to $(0, \pi/2)$, as non-zero frustration is sufficient to prevent global synchronization and avoid non-invasiveness of the coupling function. As we can see in the example in Figure 9, having non-null frustration parameters prevents global synchronization throughout time. Hence, for simplicity, for all m, we can set $\alpha^{(m)} = \alpha$.

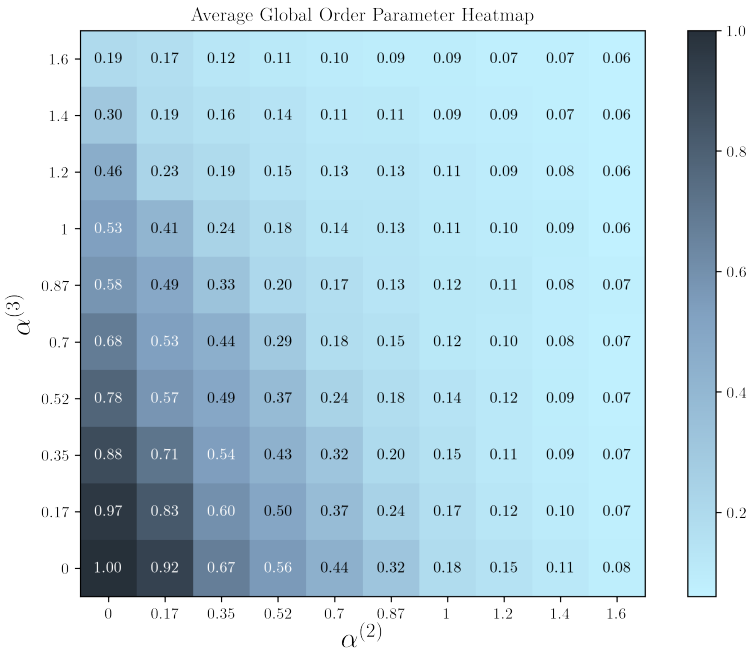

Figure 9: The average global order parameter $\langle R(t)\rangle_t$ computed over 500 time steps when changing the frustration parameters of Equation (1) with $\alpha_2, \alpha_3 \in [0, \pi/2)$. When $\langle R(t)\rangle_t$ approaches 1, it indicates near-complete phase alignment across all nodes.

We can also restate the evolution for a node i in the cluster S_a of the Kuramoto synchrony partition (Equation (1)), emphasizing the node's membership in a cluster.

$$\dot{\theta}_i = \omega_i + \sigma_2 \sum_{\beta=1}^{h} k^{(2)}_{i\,\beta} \sin\big(\theta_\beta - \theta_a - \alpha\big) + \sigma_3 \sum_{\gamma=1}^{h} \sum_{\delta=\gamma}^{h} k^{(3)}_{i\,\gamma\,\delta} \sin\big(\theta_\gamma + \theta_\delta - 2\theta_a - \alpha\big). \tag{2}$$

where the double sum with $\delta \geq \gamma$ avoids double-counting symmetric pairs of clusters in three-body interactions, after fixing an arbitrary ordering of the clusters $\{S_1, \ldots, S_h\}$. We denote $k^{(m)}_{i\,\gamma_1 \cdots \gamma_{m-1}}$ as the number of nodes sharing a hyperedge of order m with node i and belonging to the clusters specified by the remaining $m-1$ indices of k. It can be considered as the degree of the node i of order m linking i to the different subsets of clusters. We can prove the first implication by generalizing the proof of [29]. This theorem can also be simply derived from the general theory of [1, 2].

Theorem V.4 (Fibration partition ⇒ Kuramoto synchrony partition)**.** *Let $H = (N, E)$ be a connected hypergraph with rank at most 3. Consider the fibration-partition $\{C_1, \ldots, C_h\}$ of the nodes given by the fibres of the hypergraph. Then for any $\alpha \in (0, \pi/2)$, the fibration-partition is a Kuramoto synchrony partition.*

Proof. Consider a system of equations associated with the fibres C_a for $a \in \{1, \ldots, h\}$ with initial conditions $x_a(0) = x_0$ and natural frequency ω:

$$\dot{x}_a = \omega + \sigma_2 \sum_{\beta=1}^{h} k^{(2)}_{a\,\beta} \sin\big(x_\beta - x_a - \alpha\big) + \sigma_3 \sum_{\gamma=1}^{h} \sum_{\delta=\gamma}^{h} k^{(3)}_{a\,\gamma\,\delta} \sin\big(x_\gamma + x_\delta - 2x_a - \alpha\big).$$

We denote with $k^{(2)}_{a\,\beta}$ (resp. $k^{(3)}_{a\,\gamma\,\delta}$) the number of hyperedges of order 2 (resp. 3) shared by nodes in fibre C_a and C_b (resp. C_a, C_γ and C_δ). By the property of the fibration partition, all nodes $i, j \in C_a$ satisfy $k^{(m)}_{i,\beta} = k^{(m)}_{j,\beta}$ for all

β, m, which justifies the notation $k^{(m)}_{a,\beta}$ for the common value. Since the fibration partition is the coarsest equitable partition, it is not possible to have $k^{(2)}_{i\,\beta} = k^{(2)}_{j\,\beta}$ for all β if i, j are not in the same fibre. Since the evolution equation has continuous partial derivatives with respect to every x_a, by Picard theorem of existence and uniqueness of the Cauchy problem, every differential equation has a unique solution associated with the initial condition. Now consider the system of $|N|$ Equation (1). Set the same initial condition and natural frequencies for each node in the hypergraph $(\theta_i(0), \omega_i) = (x_0, \omega)$. For each node $i \in C_a$, we consider the equation:

$$\dot{\theta}_i = \omega + \sigma_2 \sum_{\beta=1}^{h} k^{(2)}_{i\,\beta} \sin\left(\theta_\beta - \theta_a - \alpha\right) + \sigma_3 \sum_{\gamma=1}^{h} \sum_{\delta=\gamma}^{h} k^{(3)}_{i\,\gamma\,\delta} \sin\left(\theta_\gamma + \theta_\delta - 2\theta_a - \alpha\right)$$

The same uniqueness argument applies here. All nodes $i \in C_a$ share the coefficients $k^{(m)}_{a,\beta}$ and thus satisfy the same ODE. Therefore, $\theta_i(t) = x_a(t)$ is the unique solution for each $a \in \{1, \dots h\}$, for all $i \in C_a$ and $t \geq 0$, i.e., all nodes in the same fibre evolve identically. □

Remark V.5. When we assign identical initial conditions to all nodes, we eliminate the case of more refined equitable partitions (EP). This is because in finer partitions, nodes that share the same input tree structure could end up in separate clusters created by the EP if the natural frequencies or the initial conditions are different. However, since these nodes follow identical evolution equations and start with the same initial conditions, they would naturally belong to the same cluster under the Kuramoto synchrony partition. This means that nodes artificially separated into different clusters would still synchronize with each other. Our objective is to identify the largest possible clusters where all nodes within each cluster achieve synchronization. Therefore, with identical initial conditions, the Kuramoto synchrony partition coincides with the coarsest equitable partition (the fibration), avoiding the degenerate case of global synchronization.

Remark V.6. Observe that nodes in the same cluster for the Kuramoto synchrony partition have the same degree for all orders. Indeed, let $S_1 \sqcup \cdots \sqcup S_j = N$ be the Kuramoto synchrony partition. Let i and j belong to the same cluster; by definition, they have the same trajectory and hence the same ODE for all $t \geq 0$. We indicate with $k^{(m)}_i$ the generalized degree of order m for node i, i.e. the number of hyperedges of order m containing the node i. Their difference equation at $t = 0$ is the following:

$$\dot{\theta}_i(0) - \dot{\theta}_j(0) = -\sin\alpha \sum_{m=2}^{3} \sigma_m (k^{(m)}_i - k^{(m)}_j) = 0.$$

Starting from the same initial conditions and natural frequencies for all nodes in the hypergraph, the only way to obtain $\dot{\theta}_i(0) = \dot{\theta}_j(0)$ for all pair of nodes $i, j \in C_a$ and independently of the $\{\sigma_m\}_m$, is to have the same degree sequence, as the frustration parameter belongs to the interval $(0, \pi/2)$. Namely:

$$k^{(m)}_i = k^{(m)}_j \;\; \forall m, \forall i, j \in C_a.$$

Since trajectories remain identical for all $t > 0$, this structural degree condition is necessary for synchrony under our dynamics.

Kirkland et al. in [29] prove that all equitable partitions in graphs are Kuramoto synchrony partitions (called α-Kuramoto partitions). However, the reverse does not always hold in their setting. Starting from initial conditions that differ for each partition, graphs can exhibit synchronization among nodes with specific degree relations, even if they do not belong to the same cluster of the equitable partition. How does this extend to hypergraphs where nodes share identical initial conditions and natural frequencies? We now prove that a Kuramoto synchrony partition for our model and homogeneous setting must coincide with a fibration partition, apart from exceptional cases. The result shows that, for generic coupling parameters, any non-fibration synchrony is destroyed instantaneously by a mismatch in incidence patterns. Only nodes with identical higher-order coupling profiles (i.e. those in the same fibre) can sustain exact synchrony.

Theorem V.7. *Consider a connected hypergraph $H = (N, E)$ with rank $rk(H) \leq 3$. For almost every choice of parameters $\alpha, \sigma_2, \sigma_3$, the synchrony partition is a Kuramoto fibration partition, except on a set of initial conditions of Lebesgue measure zero.*

Proof. Let $S_1 \sqcup \cdots \sqcup S_h = N$ be the Kuramoto synchrony partition with respect to Equation (2) with identical initial conditions and natural frequencies for all nodes (θ_0, ω_0) Take two synchronous nodes $i, j \in S_a$. By definition of synchrony partition, $\theta_i(t) = \theta_j(t) \;\; \forall t \geq 0$, which implies that their derivative must be constantly equal

$$\dot{\theta}_i(t) = \dot{\theta}_j(t) \;\; \forall t \geq 0.$$

Consider the evolution of the nodes. Using the cluster representation θ_β for the common phase of all nodes in cluster S_β, we write:

$$\dot{\theta}_i = \omega_0 + \sigma_2 \sum_{\beta=1}^{h} k_{i\,\beta}^{(2)} \sin\big(\theta_\beta - \theta_a - \alpha\big) + \sigma_3 \sum_{\gamma=1}^{h} \sum_{\delta=\gamma}^{h} k_{i\,\gamma\,\delta}^{(3)} \sin\big(\theta_\gamma + \theta_\delta - 2\theta_a - \alpha\big)$$

$$\dot{\theta}_j = \omega_0 + \sigma_2 \sum_{\beta=1}^{h} k_{j\,\beta}^{(2)} \sin\big(\theta_\beta - \theta_a - \alpha\big) + \sigma_3 \sum_{\gamma=1}^{h} \sum_{\delta=\gamma}^{h} k_{j\,\gamma\,\delta}^{(3)} \sin\big(\theta_\gamma + \theta_\delta - 2\theta_a - \alpha\big)$$

where the double sum with $\delta \geq \gamma$ avoids double-counting three-body interactions, after fixing an order for the clusters $\{S_1, \ldots, S_h\}$. Their difference $\theta_{ij} := \theta_i - \theta_j$ vanishes for all t. For ease of notation, we omit the dependence of θ on t.

$$\dot{\theta}_{ij} = \sigma_2 \sum_{\beta=1}^{h} (k_{i\,\beta}^{(2)} - k_{j\,\beta}^{(2)}) \sin\big(\theta_\beta - \theta_a - \alpha\big) + \sigma_3 \sum_{\gamma=1}^{h} \sum_{\delta=\gamma}^{h} (k_{i\,\gamma\,\delta}^{(3)} - k_{j\,\gamma\,\delta}^{(3)}) \sin\big(\theta_\gamma + \theta_\delta - 2\theta_a - \alpha\big)$$

Since all nodes start with identical initial conditions θ_0, we have $\theta_\beta(0) = \theta_a(0)$ for all S_a, S_β. For the sine terms to vanish identically, one would need:

$$\theta_\beta(t) - \theta_a(t) \in \{\alpha + 2\pi\mathbb{Z}\} \quad \text{or} \quad \theta_\beta(t) - \theta_a(t) \in \{\pi - \alpha + 2\pi\mathbb{Z}\},$$

and similarly

$$\theta_\gamma(t) + \theta_\delta(t) - 2\theta_a(t) \in \{\alpha + 2\pi\mathbb{Z}\} \quad \text{or} \quad \theta_\gamma(t) + \theta_\delta(t) - 2\theta_a(t) \in \{\pi - \alpha + 2\pi\mathbb{Z}\}.$$

Such constant phase differences are incompatible with identical initial conditions unless they vanish trivially; hence, for a generic trajectory, these sine terms do not vanish identically.

Now, define the function

$$F_{ij}(\Theta, p) := \sigma_2 \sum_{\beta=1}^{h} (k_{i\,\beta}^{(2)} - k_{j\,\beta}^{(2)}) \sin\big(\theta_\beta - \theta_a - \alpha\big) + \sigma_3 \sum_{\gamma=1}^{h} \sum_{\delta=\gamma}^{h} (k_{i\,\gamma\,\delta}^{(3)} - k_{j\,\gamma\,\delta}^{(3)}) \sin\big(\theta_\gamma + \theta_\delta - 2\theta_a - \alpha\big).$$

where $\Theta = (\theta_1, \ldots, \theta_{|N|}) \in \mathbb{T}^{|N|} = [0, 2\pi)^{|N|}$, and $p = (\alpha, \sigma_2, \sigma_3)$. F_{ij} is real analytic on $\mathbb{T}^{|N|}$ as a finite sum of sines of linear combinations of phase variables.

If at least one incidence difference $k_{i\beta}^{(2)} - k_{j\beta}^{(2)}$ or $k_{i\gamma\delta}^{(3)} - k_{j\gamma\delta}^{(3)}$ is non–zero, then F_{ij} is not identically zero. By a classical result on analytic functions [41], a non-identically zero real-analytic function on a compact domain has a zero set of Lebesgue measure zero. Hence, the zero set $Z_{ij}(p) := \{\Theta \in \mathbb{T}^{|N|} : F_{ij}(\Theta, p) = 0\}$ has measure 0 for generic parameters p. Since the trajectory $\Theta(t)$ evolves continuously and deterministically from initial condition $\Theta(0)$, requiring $\Theta(t) \in Z_{ij}(p)$ for all $t \geq 0$ means the trajectory must remain confined to a measure-zero subset of the phase space. The set of initial conditions generating such trajectories has measure zero: if $\Theta(0) \notin Z_{ij}(p)$, then by continuity $\Theta(t) \notin Z_{ij}(p)$ for at least a small time interval, violating synchrony. Therefore, synchrony between nodes i and j that are not in the same fibre can only occur for initial conditions forming a set of measure zero.

If all incidence differences vanish,

$$k_{i,\beta}^{(2)} = k_{j,\beta}^{(2)}\ \forall\beta, \qquad k_{i,\gamma,\delta}^{(3)} = k_{j,\gamma,\delta}^{(3)} \quad \forall(\gamma, \delta),$$

then i and j belong to the same fibre by definition.

For generic parameters and almost all initial conditions, synchrony occurs only between nodes in the same fibre. □

Remark V.8. The emergence of synchronization is governed not only by the presence of connections but also by the organization of interactions into fibres, subsets of nodes that share equivalent dynamical roles. These fibres are not intrinsic to the node set alone; they depend on how the system is represented. A hypergraph, its projection to a simple graph, or a multiedge graph can each induce different fibre structures as exemplified in Figure 4. The two previous theorems show that it has a direct impact on which groups of nodes synchronize, starting from the same initial conditions. Only clusters that align with the true fibre structure of the interaction model can be expected to maintain internal coherence. If an incorrect or oversimplified representation is used, synchronization is lost. This phenomenon is illustrated in Figure 10, where the same dynamical system is represented as a hypergraph (top row), a simple graph (middle), and a multiedge graph (bottom), with reference to Figure 4. Although the parameters and initial conditions are identical, different sets of nodes synchronize in each case, corresponding to the different fibres. The set of represented nodes $[1, 2, 4, 5, 8, 9]$ is split into three different fibres for the hypergraph, a unique fibre for the graph, and two fibres for the multigraph. This structural condition coincides with the dynamical condition of cluster synchronization.

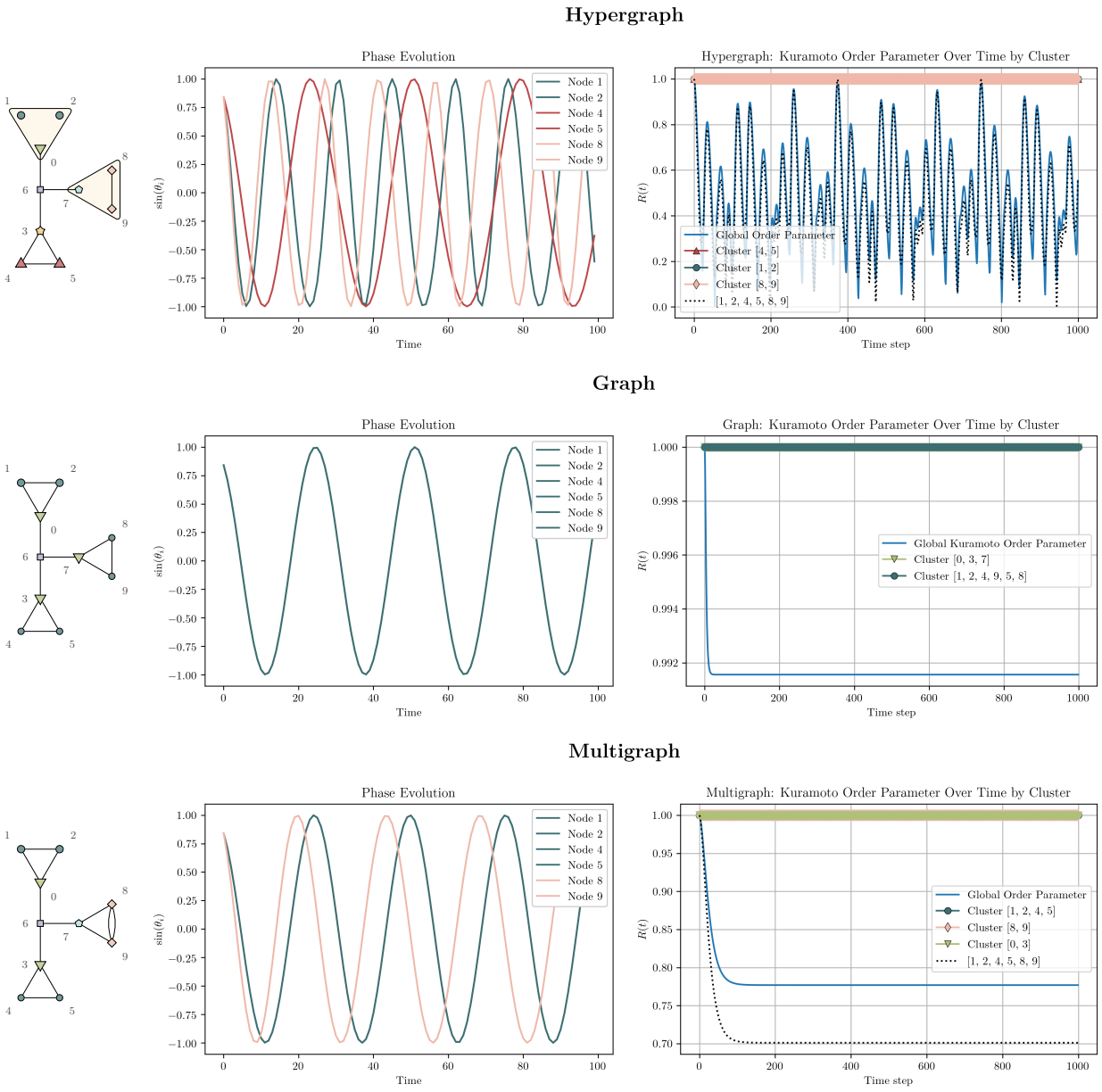

Figure 10: Comparison of the dynamics of the higher-order Kuramoto model with frustration for the example shown in Figure 4 across three different representations reported on the left of the plots: the hypergraph (top row), its projection in a simple graph (middle row), and its projection in a graph with multiple edges (bottom row). The left plot shows the sine of the phase evolution over the first 100 time steps for the selected nodes $[1, 2, 4, 5, 8, 9]$ that change fibre depending on the representation, colored according to the fibre they belong to. The right plot reports the local Kuramoto order parameter $R(t)$, measuring phase coherence within each fibre. Colored lines represent intra-fibre synchronization, and the blue thin line shows the global order parameter. For the hypergraph and the multi-order graph (lines 1 and 3), we also report with the dotted black line the measure of coherence computed for the subset of nodes $[1, 2, 4, 5, 8, 9]$ (which is a fibre only for the simple graph) to illustrate different synchronization patterns across different representations. On the right, the intra-fibre local order parameters are completely overlapped as they are identically 1. This highlights how synchronization patterns can vary significantly depending on the chosen representation. The parameters for the dynamic Equation (2) have initial condition and natural frequencies $(\theta_i, \omega_i) = (1, 0)$ for all nodes i, frustration parameter $\alpha = \pi/6$, and the strength parameters are $(\sigma_2, \sigma_3) = (0.2, 0.8)$

Algorithm for synchronized nodes

Through the previous theoretical analysis, we established a correspondence between hypergraph fibres and synchronizing nodes within a higher-order Kuramoto model incorporating frustration parameters. To empirically verify this relationship, we developed Algorithm 2 that groups nodes based on phase coherence measures. In Theorem V.6, we note that nodes with identical initial conditions and natural frequencies will synchronize if they share the same degree at every order, so initially we categorize them as such. The algorithm then involves temporal sampling by comparing phases pairwise among node combinations within the same split (with the same degree for all orders). For node pairs with aligned phases at all sampled times, we compute the average local order parameter over time to identify nearly unitary values as synchronized clusters. These pairwise clusters were subsequently merged when sharing common elements, resulting in a partitioning of the nodes. To efficiently merge these pairwise synchronized clusters when they share common nodes, we construct an undirected graph where each node represents a Kuramoto oscillator, and edges connect those found to be pairwise synchronized. The connected components of this support graph correspond to the final synchronized clusters. The experimental results, validated across both real-world datasets and synthetic hypergraphs, reproduced the theoretical predictions of the fibres. Kuramoto-based clustering methodologies have been extensively investigated in the literature, with notable contributions (e.g. [42, 43]). Specifically, we can state that when employing a Kuramoto model with identical initial conditions and natural frequencies across all nodes, and non-zero frustration parameters, global synchronization is inhibited. In contrast, local synchronization emerges among nodes that share equivalent inflow information structures.

Algorithm 2: Extracting synchronized clusters from HO Kuramoto with frustration dynamics.

Input: Phase history matrix $\Theta \in \mathbb{R}^{T\times|N|}$, node groups $\{N_d\}_d$ by sequence of degree for all hyperedges orders, tolerance $\epsilon > 0$, number of time samples n.
Output: Set of synchronized clusters $C = \{C_1, \ldots, C_m\}$.
Step 1: Sample time points.
Randomly select n time indices $\{t_1, \ldots, t_n\}$ from $\{1, \ldots, T\}$.
Step 2: Iterate over degree-based node groups.
foreach *group of nodes* $V_d = N_d$ **do**
  Initialize a graph G_d with node set V_d.
  foreach *pair* $(i, j) \in V_d \times V_d$ **do**
    Extract trajectories $\theta_i(t)$ and $\theta_j(t)$ from Θ.
    if $|\theta_i(t_k) - \theta_j(t_k)| < \epsilon$ *for all* $k = 1, \ldots, n$ **then**
      Compute the average order parameter $\langle R_{ij}\rangle$ over all time.
      if $\langle R_{ij}\rangle < \epsilon$ **then**
        Add edge (i, j) to G_d.
      end
    end
  end
  Step 3: Extract synchronized clusters.
  Compute connected components $\{C_1^{(d)}, \ldots, C_{m_d}^{(d)}\}$ of G_d.
  foreach $C_\ell^{(d)}$ **do**
    Add $C_\ell^{(d)}$ to C.
  end
end
return C *(maximal synchronized clusters).*

Remark V.9. Up to this point, our analysis has focused on the emergence of clustered dynamics in the Kuramoto model with frustration and both two and three-body interactions, starting from identical initial conditions and natural frequencies for all nodes. This setting guarantees intra-cluster cohesion, as nodes within the same fibre evolve identically, but inhibits global synchronization thanks to the presence of frustration parameters. We now turn to the complementary question: given the same initial conditions, how should natural frequencies be adjusted to preserve consistency within fibres while achieving global frequency synchronization across all clusters? The answer is elaborated in Section B, and the answer turns out to be related not directly to fibres but to the more general degrees of all orders.

VI. MODIFYING TOPOLOGY TO RECOVER OR ENFORCE SYMMETRIES

The role of symmetry in network science has evolved from a purely descriptive framework, centered on automorphisms and equitable partitions, to a tool for designing and repairing networked systems to achieve desired dynamical behavior. Recent advances have emphasized two intertwined goals: the recovery of symmetries in networks distorted by noise, incomplete data, or broken connectivity, and the engineering of symmetries through minimal topological interventions to guide or enhance processes such as synchronization or control. These efforts reveal symmetry not merely as an inherent property, but as a target of intervention, bridging structural analysis and dynamical optimization.

This section provides an overview of recent contributions in this paradigm. Each approach addresses the challenge of how to modify a network to reflect or enforce a desired symmetry, whether derived from observed dynamics, known structural constraints, or theoretical design goals. Introducing a rigorous framework to approach the problem, Boldi et al. [17] define the notion of quasifibrations as a way to recover approximate symmetries in biological networks by identifying minimal modifications to the topology that restore an underlying fibration-like structure. Similarly, Leifer et al. [19] develop a symmetry-driven network reconstruction method that modifies edges to satisfy local balance constraints based on pseudocoloring, offering an approach to repair corrupted networks and obtain the optimized number of clusters. In a different direction, Gambuzza et al. [18] focus on enforcing desired symmetries to achieve clustered dynamics, proposing targeted topological interventions based on external equitable partitions that guarantee stable cluster synchronization. Other works adopt generative or learning-based approaches: Klickstein and Sorrentino [44] construct synthetic networks with predefined automorphism groups to serve as symmetry benchmarks, while Zou et al. [45] use reinforcement learning with graph neural networks to rewire network links and achieve symmetry patterns that support cluster synchronization. Closing the loop between theory and application, Zou et al. [46] show how structural symmetry can be leveraged in physical systems to control chaotic synchronization, proving that altering a network to match dynamical symmetry is both theoretically justified and experimentally feasible. Together, these contributions (see the comparative Table II) highlight a growing perspective where symmetries are not only analysed but also shaped or repaired, providing a natural foundation for extending these ideas to hypergraphs, where higher-order symmetries can be studied through generalized fibrations. The field of hypergraph modifications for symmetry analysis raises many questions and provides directions for future research.

Work	**Target problem**	**Mathematical object**	**Main technique**
Boldi et al. (2022) [17]	Recover latent symmetries from incomplete graphs	Quasifibration	Greedy and local isomorphism checks
Gambuzza et al. (2021) [18]	Impose a target cluster pattern	Balanced Laplacian perturbation	Mixed-integer and convex optimisation
Klickstein et al. (2018) [44]	Produce test graphs with chosen symmetry	Automorphisms and equitable partitions	Constructive group-theoretic generator
Leifer et al. (2022) [19]	Repair noisy networks via pseudosymmetries	Pseudobalanced colouring	Integer programming
Zou et al. (2024) [45]	Learn rewiring policy for achievable cluster sync	Graph Convolution Network	Deep reinforcement learning

Table II: Comparison of some recent approaches for recovering or enforcing network symmetries.

In what follows, we make an initial contribution by tackling challenges arising from realistic data scenarios and computational constraints: reconstructing latent symmetries from partial observations and eliminating structural redundancy, maintaining equivalence relationships for information flows. Figure 11 recaps with three simple examples the problems.

A. Sparsification of a hypergraph preserving fibres

We address a problem related to higher-order interactions in network modification for the recovery or enforcement of symmetry. As already observed, hypergraphs represent systems with multi-node interactions, such as social groups, biochemical reactions, or communication networks. These often contain redundant hyperedges that contribute little to distinguish nodes having different information flows. Removing such redundancies simplifies the hypergraph, improves interpretability, and speeds up analysis and simulation. We seek a process that preserves connectivity, avoids adding new connections, and maintains fibre structures. Starting from a hypergraph, we aim to find a connected hypergraph

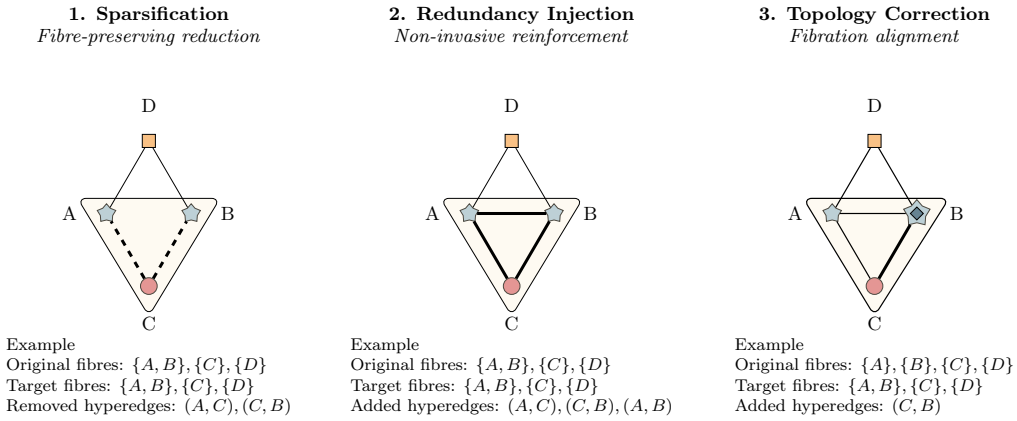

Figure 11: Examples of hypergraph modifications aimed at: (1) reducing or (2) increasing the redundancy of informative hyperedges while preserving the original fibre partition of the nodes. Case (3) illustrates the addition of hyperedges to achieve a target fibre partition. Dashed hyperedges represent those removed by the algorithm, while thick hyperedges indicate additions made to enforce a specific input configuration on the nodes.

having the same nodes as the original and with the minimum number of hyperedges needed to preserve the partition of the nodes induced by the fibration symmetry.

Algorithmic approach When partitioning the nodes in fibres with Algorithm 1, a color is also assigned to each hyperedge, based on the fibres of the nodes belonging to it. Then, Algorithm 3 exploits this coloring scheme and applies a greedy, iterative process to remove these hyperedge classes one by one, accepting removals only when they preserve the fibre partition and connectivity. To explore the solution space, it tests multiple random permutations of the order in which hyperedge classes are removed, retaining the sparsification that yields the smallest hyperedge set while meeting constraints. Additionally, in a variant of the algorithm, it is possible to specify a set of hyperedges that must not be removed, either because their presence is experimentally validated or because they are known to be structurally critical. In this case, the sparsification procedure is constrained to preserve those hyperedges. While the greedy approach is computationally efficient for large hypergraphs, it does not guarantee a globally optimal solution; hence, the minimal possible hyperedge set preserving fibres and connectivity may not be found. This limitation arises because decisions are made sequentially without backtracking or exhaustive search, potentially missing better combinations of removals. However, the method combines feasibility and structural consistency, providing a sparsification that respects fibration symmetries and connectivity, which is sufficient for many applications.

Algorithm 3: Greedy sparsification of a hypergraph while preserving fibre partitions and connectivity.

Input: Hypergraph $H = (N, E)$ and a node partition $C = \{C_i\}$ representing fibres.
Output: A reduced hypergraph $H' = (N, E')$ with $|E'| \leq |E|$ preserving both fibre structure and connectivity.
Step 1: Group hyperedges by structural color.
Group hyperedges that share the same color obtained with Algorithm 1.
Step 2: Generate candidate color removal orders.
Define several orders in which to attempt removing hyperedge color groups.
Step 3: Iteratively attempt to remove hyperedges.
foreach *color group in the selected order* **do**
  Temporarily remove all hyperedges of this color group.
  if *the resulting hypergraph is connected and the fibre partition preserved* **then**
    Accept the removal permanently.
  end
  else
    Roll back the removal.
  end
end
Step 4: Return the sparsified hypergraph.
Among all the sets of new hyperedges computed in Step 3 in correspondence of different color orders, keep the smallest E'.

B. Modifying hypergraphs to match target fibres

In this work, we have observed that nodes belonging to the same fibre often exhibit synchronization or tightly correlated behavior, as predicted by the underlying local symmetries of the hypergraph. However, in real-world or biological systems, the observed topology may be incomplete or corrupted due to measurement noise, data loss, or partial observation. As a result, the hypergraph topology might not reflect the true interaction structure responsible for the observed dynamical patterns. When we observe (or can deduce) that specific nodes exhibit synchronized or identical behavior, we can leverage this information to reconstruct a likely hypergraph structure. This reconstructed hypergraph would reproduce the observed pattern of synchronized node groups while maintaining maximum similarity to the original network's structure and dynamics.

Algorithmic approach The approach we propose in Algorithm 4 is greedy and heuristic, relying on iterative adjustments. Initially, we iteratively compare the actual fibres and the target fibres after adding new hyperedges. Then we use a version of the pruning Algorithm 3 to reduce the number of hyperedges while keeping the original hyperedges in E: in this way, we avoid removing original hyperedges. Since the process depends on incremental structural corrections, convergence is not guaranteed, especially for complex or conflicting target partitions.

Algorithm 4: Modification of a hypergraph to reach target fibre partition.

Input: Hypergraph $H = (N, E)$ and a target fibre partition $C = \{C_i\}$.
Output: A hypergraph $H' = (N, E')$ with fibre structure C.
Step 1: Initialization.
Compute P, the fibre partition of H.
Step 2: Refine the fibre structure.
while *P differs from C and iteration limit not reached* **do**
  Compute current fibre partition P.
  foreach *cluster in $P \setminus C$* **do**
    Add minimal differences to split the cluster.
  end
  foreach *cluster in $C \setminus P$* **do**
    Add minimal common connectivity to merge the cluster.
  end
end
Step 3: Sparsify the hypergraph.
Apply Algorithm 3 to remove redundant hyperedges not removing original hyperedges in E while preserving C and connectivity.
Step 4: Return final result.
Output the resulting hypergraph (N, E').

C. Adding redundant hyperedges without altering fibres

While minimizing the number of hyperedges is often desirable, strategically adding redundancy can reinforce symmetries, preserve fibre structure, and improve the functional and dynamical properties of the hypergraph without altering the essential partition, enhancing robustness to perturbations and enabling more regular, compressible representations that facilitate analysis and model reduction.

Algorithmic approach The method described in Algorithm 5 adds new hyperedges in a way that reinforces a given fibre partition C while preserving it. The procedure is structural and randomized: it samples combinations of clusters and generates new hyperedges by connecting nodes from those clusters. To ensure consistency, the number of new hyperedges added at each step is the least common multiple of the sizes of the selected clusters, and nodes are paired cyclically. In this way, we do not disrupt the connection coherence intra-cluster. In detail, at each iteration, the algorithm selects a target hyperedge order r from a pre-shuffled list of integers. This shuffling ensures a fair exploration of interaction orders, avoiding any systematic bias toward lower or higher orders. To construct a candidate set of hyperedges, the algorithm randomly picks r distinct clusters from the partition C, where r is the chosen order. Importantly, it may not be enough to add a single hyperedge: to preserve the fibre structure, all nodes within each selected cluster must receive identical new connection patterns. This guarantees that their structural role in the hypergraph remains symmetric. To enforce this uniformity, the algorithm computes the least common multiple L of the sizes of the selected clusters. This value determines the number of hyperedges to generate. For each cluster, its nodes are sampled without replacement and then repeated cyclically until a list of length L is formed. These repeated lists are then zipped together with one node from each list per position, to produce exactly L hyperedges. Each of

these new hyperedges connects one node from each selected cluster, ensuring that every node in those clusters appears the same number of times across the batch. The result is a structurally consistent set of interactions that respects the symmetries encoded by C. Each batch of candidate hyperedges is accepted only if the resulting hypergraph preserves the original fibre partition. Indeed, even if the addition of hyperedges to maintain the same kind and number of connections intra-fibre is preserved, some clusters may collapse and unite into a single, larger fibre. This procedure allows the hypergraph to gain structural redundancy while strictly maintaining the predefined node grouping.

Algorithm 5: Addition of redundant hyperedges preserving a target fibre partition.

Input: Hypergraph $H = (N, E)$ with fibre partition $C = \{C_i\}$, maximum number of hyperedges to add K, maximum number of iterations T.
Output: A hypergraph $H' = (N, E')$ with $|E'| \geq |E|$ preserving both fibre structure C.
Step 1: Initialization.
Let $E' \leftarrow E$ be the set of current hyperedges.
Let $d = rk(H)$.
Initialize a counter for added hyperedges.
Let T be the total number of trials (iteration limit).
Define a random sequence over orders $2, \ldots, d$.
Step 2: Iteratively attempt to add new hyperedges.
while *number of added hyperedges* $< K$ *and trials left* **do**
  Pick order r from the random sequence.
  Randomly select r distinct clusters from C.
  for $i \leftarrow 1$ *to* 3 *(retry limit)* **do**
    Compute the least common multiple L of the sizes of the selected clusters.
    For each cluster C_i, sample its nodes without replacement and repeat them cyclically to reach length L.
    Construct L candidate hyperedges by zipping together one node from each repeated cluster list.
    if *none of the candidate hyperedges already exist in* E' **then**
      Temporarily add them to form E''.
      if *fibre partition of* $H'' = (N, E'')$ *equals* C **then**
        Commit $E' \leftarrow E''$.
        Update the counter of added hyperedges.
        break retry loop.
      end
    end
  end
end
Step 3: Return final result.
Output the resulting hypergraph $H' = (N, E')$.

VII. CONCLUSIONS

In this work, we have explored the relationship between structural symmetries in hypergraphs and the emergence of synchronization patterns in dynamical systems. We have deepened the understanding of fibration symmetry for complex systems with higher-order interactions, using the frustrated Kuramoto model as an example to study the dependence of topology on the emergence of cluster synchronization patterns. However, our theoretical framework relies on a critical assumption that significantly limits its direct applicability to real-world processes: the requirement of identical initial conditions and natural frequencies across all nodes. This assumption, while mathematically necessary for our theoretical results, is unrealistic in natural systems. Real networks invariably exhibit heterogeneity in both initial states and intrinsic dynamics, making our exact synchrony conditions often unattainable. Despite these limitations, the duality between structural fibration and dynamical synchronization revealed through the Kuramoto framework provides valuable theoretical insights. It offers alternatives for algorithmic applications in clustering and community detection. The Kuramoto model's ability to naturally organize nodes according to underlying structural symmetries suggests potential when considering frustration parameters to inhibit global synchronization. For practical relevance, we suggest greedy hypergraph compression methods that keep fibration compatibility and employ topology modification strategies to achieve desired node partitions, useful for handling incomplete or noisy data. Future work could explore generalizations of the framework introduced here, including the development of enhanced algorithms beyond the greedy approaches presented here for topology modification problems. Such extensions help capture more nuanced forms of partial synchronization in systems where the exact fibre structure is absent.

[1] M. Aguiar, C. Bick, and A. Dias, Nonlinearity **36**, 4641 (2023).
[2] S. von der Gracht, E. Nijholt, and B. Rink, SIAM Journal on Applied Mathematics **83**, 2329 (2023).
[3] R. Brown, Bulletin of The London Mathematical Society - BULL LOND MATH SOC **19**, 113 (1987), version consulted: April 2, 2012 with some corrections to previous latexed versions and some updates on the references.
[4] A. Grothendieck, in *Séminaire Bourbaki : Années 1958/59 - 1959/60, Exposés 169-204*, Astérisque No. 5 (Société mathématique de France, 1960) pp. 299–327.
[5] P. Boldi and S. Vigna, Discrete Mathematics **243**, 21 (2002).
[6] L. Deville and E. Lerman, Journal of the European Mathematical Society **17** (2013).
[7] E. Nijholt, B. Rink, and J. Sanders, Journal of Differential Equations **261**, 4861 (2016).
[8] F. Battiston, G. Cencetti, I. Iacopini, V. Latora, M. Lucas, A. Patania, J. G. Young, and G. Petri, Physics Reports **874**, 1 (2020), 2006.01764.
[9] C. Bick, E. Gross, H. A. Harrington, and M. T. Schaub, SIAM Review **65**, 686 (2023).
[10] P. Boldi, in *2023 IEEE 9th International Conference on Collaboration and Internet Computing (CIC)* (2023) pp. 1–7.
[11] A. Salova and R. M. D'Souza, Cluster synchronization on hypergraphs (2022), arXiv:2101.05464 [cond-mat, physics:nlin].
[12] H. A. Makse, P. Boldi, F. Sorrentino, and I. Stewart, Symmetries of Living Systems: Symmetry Fibrations and Synchronization in Biological Networks (2025), arXiv:2502.18713 [q-bio].
[13] V. Nicosia, M. Valencia, M. Chavez, A. Díaz-Guilera, and V. Latora, Phys. Rev. Lett. **110**, 174102 (2013).
[14] Y. Zhang, P. S. Skardal, F. Battiston, G. Petri, and M. Lucas, Science Advances **10**, eado8049 (2024).
[15] Y. Zhang, M. Lucas, and F. Battiston, Nature Communications **14**, 1605 (2023).
[16] A. Salova and R. M. D'Souza, Analyzing states beyond full synchronization on hypergraphs requires methods beyond projected networks (2021), arXiv:2107.13712 [cond-mat, physics:nlin].
[17] P. Boldi, I. Leifer, and H. A. Makse, Journal of Statistical Mechanics: Theory and Experiment **2022**, 113401 (2022).
[18] L. V. Gambuzza, M. Frasca, F. Sorrentino, L. M. Pecora, and S. Boccaletti, IEEE Transactions on Network Science and Engineering **8**, 282 (2021).
[19] I. Leifer, D. Phillips, F. Sorrentino, and H. A. Makse, Journal of Statistical Mechanics: Theory and Experiment **2022**, 073403 (2022).
[20] I. Leifer, M. Sánchez-Pérez, C. Ishida, and H. A. Makse, BMC Bioinformatics **22**, 10.1186/s12859-021-04213-5 (2021).
[21] F. Morone and H. A. Makse, Nature Communications **10**, 10.1038/s41467-019-12675-8 (2019).
[22] M. Golubitsky and I. Stewart, Bulletin of the American Mathematical Society **43**, 305 (2006).
[23] H. Makse, T. Gili, B. Avila, L. Pasquini, A. Holodny, D. Phillips, P. Boldi, A. Gabrielli, G. Caldarelli, and M. Zimmer, Fibration symmetry-breaking supports functional transitions in a brain network engaged in language (2024).
[24] H. Kamei and P. J. A. Cock, SIAM Journal on Applied Dynamical Systems **12**, 352 (2013), 1211.6334 [math].
[25] Y. Zhang, V. Latora, and A. E. Motter, Communications Physics **4**, 1 (2021).
[26] L. V. Gambuzza, F. Di Patti, L. Gallo, S. Lepri, M. Romance, R. Criado, M. Frasca, V. Latora, and S. Boccaletti, Nature Communications **12**, 1255 (2021).
[27] L. M. Pecora, F. Sorrentino, A. M. Hagerstrom, T. E. Murphy, and R. Roy, Nature Communications **5**, 10.1038/ncomms5079 (2014).
[28] M. Schaub, N. O'Clery, Y. Billeh, J.-C. Delvenne, R. Lambiotte, and M. Barahona, Chaos: An Interdisciplinary Journal of Nonlinear Science **26**, 10.1063/1.4961065 (2016).
[29] S. Kirkland and S. Severini, Applicable Analysis and Discrete Mathematics **9**, 10.2298/AADM141124018K (2013).
[30] M. Brede and A. C. Kalloniatis, Phys. Rev. E **93**, 062315 (2016).
[31] S. Dutta, A. Mondal, P. Kundu, P. Khanra, P. Pal, and C. Hens, Phys. Rev. E **108**, 034208 (2023).
[32] B. Moyal, P. Rajwani, S. Dutta, and S. Jalan, Phys. Rev. E **109**, 034211 (2024).
[33] I. León, R. Muolo, S. Hata, and H. Nakao, Chaos: An Interdisciplinary Journal of Nonlinear Science **34**, 013105 (2024).
[34] L. Gallo, R. Muolo, L. V. Gambuzza, V. Latora, M. Frasca, and T. Carletti, Communications Physics **5**, 1 (2022).
[35] F. Morone, I. Leifer, and H. A. Makse, Proceedings of the National Academy of Sciences **117**, 8306 (2020).
[36] N. W. Landry, M. Lucas, I. Iacopini, G. Petri, A. Schwarze, A. Patania, and L. Torres, Journal of Open Source Software **8**, 5162 (2023).
[37] I. Amburg, N. Veldt, and A. Benson, in *Proceedings of The Web Conference 2020*, WWW '20 (Association for Computing Machinery, New York, NY, USA, 2020) p. 706–717.
[38] A. Sinha, Z. Shen, Y. Song, H. Ma, D. Eide, B.-J. P. Hsu, and K. Wang, in *Proceedings of the 24th International Conference on World Wide Web*, WWW '15 Companion (Association for Computing Machinery, New York, NY, USA, 2015) pp. 243–246.
[39] R. Muolo, H. Nakao, and M. Coraggio, When higher-order interactions enhance synchronization: The case of the Kuramoto model (2025), arXiv:2508.10992 [nlin].
[40] K.-I. Goh, M. E. Cusick, D. Valle, B. Childs, M. Vidal, and A.-L. Barabási, Proceedings of the National Academy of Sciences **104**, 8685 (2007).
[41] B. Mityagin, The Zero Set of a Real Analytic Function (2015), arXiv:1512.07276 [math].
[42] C. Böhm, C. Plant, J. Shao, and Q. Yang, in *Proceedings of the 16th ACM SIGKDD International Conference on Knowledge Discovery and Data Mining*, KDD '10 (Association for Computing Machinery, New York, NY, USA, 2010) pp. 583–592.

[43] J. Shao, X. He, Q. Yang, C. Plant, and C. Böhm, in *Advances in Knowledge Discovery and Data Mining*, edited by J. Pei, V. S. Tseng, L. Cao, H. Motoda, and G. Xu (Springer, Berlin, Heidelberg, 2013) pp. 249–260.
[44] I. Klickstein and F. Sorrentino, Chaos (Woodbury, N.Y.) **28**, 121102 (2018).
[45] M. Zou, W. Guo, and K.-F. Chu, IEEE Transactions on Network Science and Engineering **11**, 4293 (2024).
[46] T. Zou, W. Pan, C. Hu, S. Li, L. Yan, B. Luo, X. Zou, and L. Zhang, Optics Express **33**, 28243 (2025).
[47] S. Dutta, P. Kundu, P. Khanra, C. Hens, and P. Pal, Phys. Rev. E **108**, 024304 (2023).
[48] S. Dutta, P. Kundu, P. Khanra, C. Hens, and P. Pal, Phys. Rev. E **110**, 064317 (2024).
[49] J. L. Ocampo-Espindola, C. Bick, A. E. Motter, and I. Z. Kiss, Science Advances **11**, eadu4114 (2025).

Appendix A: Categorical equivalence

In this section, we prove the categorical equivalence between bipartite graphs and hypergraphs. Given a category C, we indicate its objects with $Ob(C)$ and its morphisms as $Mor(C)$ or $Mor_C(A, B)$ if we need to specify source objects A and target objects B.

Definition A.1 (**Hyper**)**.** The category **Hyper** has as objects the hypergraphs as defined in Theorem III.3. A morphism $f \in \mathrm{Mor}(\mathbf{Hyper})$ between two hypergraphs $H_1 = (N_1, E_1)$ and $H_2 = (N_2, E_2)$ is a pair of maps $f = (f_N, f_E) : H_1 \to H_2$, where $f_N : N_1 \to N_2$ and $f_E : E_1 \to E_2$, that satisfy:

$$v \in e \implies f_N(v) \in f_E(e)$$

for all $v \in N_1$ and $e \in E_1$. Hence, morphisms are maps between hypergraphs that send nodes to nodes and hyperedges to hyperedges, preserving the incidence relation.

Definition A.2 (**BiparGraph**)**.** The category **BiparGraph** has as objects the bipartite graphs as defined in Theorem III.7. A morphism between two bipartite graphs $G_A = (V_{A_1} \sqcup V_{A_2}, E_A)$ and $G_B = (V_{B_1} \sqcup V_{B_2}, E_B)$ is a triple of maps $f = (f_1, f_2, f_E)$ where:

- $f_1 : V_{A_1} \to V_{B_1}$
- $f_2 : V_{A_2} \to V_{B_2}$
- $f_E : E_A \to E_B$ defined by $f_E((v, u)) = (f_1(v), f_2(u))$

and $(v, u) \in E_A \;\Rightarrow\; (f_1(v), f_2(u)) \in E_B$. Hence, morphisms are maps between bipartite graphs that send nodes of the first (resp. second) layer to nodes of the first (resp. second) layer, preserving adjacency.

Definition A.3 (Functor)**.** Given two categories C, D, a functor $F : C \to D$ is a map that:

- $\forall x \in \mathrm{Ob}(C) \Rightarrow F\,x \in \mathrm{Ob}(D)$.
- If $f \in \mathrm{Mor}(C)$, $f : X \to Y$ with $X, Y \in \mathrm{Ob}(C)$, then $F\,f : F\,X \to F\,Y$ is a morphism of D such that:
  - $F\,\mathrm{id}_X = \mathrm{id}_{F\,X} \quad \forall X \in \mathrm{Ob}(C)$,
  - $F(f \circ g) = F\,f \circ F\,g \quad \forall f : X \to Y,\, g : Y \to Z$ with $X, Y, Z \in \mathrm{Ob}(C)$.

Definition A.4 (Categorical equivalence)**.** Two categories C, D are equivalent if there exists a functor $F : C \to D$ such that:

- F is full: $\forall c_1, c_2 \in \mathrm{Ob}(C)$, the map $\mathrm{Mor}_C(c_1, c_2) \longrightarrow \mathrm{Mor}_D(F\,c_1, F\,c_2)$ induced by F is surjective.
- F is faithful: $\forall c_1, c_2 \in \mathrm{Ob}(C)$, the map $\mathrm{Mor}_C(c_1, c_2) \longrightarrow \mathrm{Mor}_D(F\,c_1, F\,c_2)$ induced by F is injective.
- F is dense (essentially surjective): $\forall d \in \mathrm{Ob}(D)$, $\exists c \in \mathrm{Ob}(C)$ such that $d \cong F\,c$ (i.e., d is isomorphic to $F\,c$).

Theorem A.5. *The categories* **Hyper** *and* **BiparGraph** *are equivalent.*

Proof. We construct a functor $F : \mathbf{Hyper} \to \mathbf{BiparGraph}$ and prove it satisfies the conditions in Theorem A.4.
Functor definition:

On objects: Given a hypergraph $H = (N, E)$, define the bipartite graph

$$F\,H \coloneqq (N \sqcup E, A_H)$$

where $A_H = \{(v, e) \mid v \in N, e \in E, v \in e\}$.

On morphisms: Given a hypergraph morphism $g = (g_N, g_E) : H_1 \to H_2$, define

$$F\,g \coloneqq (g_N, g_E, g_A)$$

where $g_A((v,e)) = (g_N(v), g_E(e))$ for $(v,e) \in A_{H_1}$.

Verification that F is a functor:

Preserves identities: For any hypergraph H, $F(\mathrm{id}_H) = (\mathrm{id}_N, \mathrm{id}_E, \mathrm{id}_{A_H}) = \mathrm{id}_{F\,H}$.

Preserves composition: For morphisms $g_1 : H_1 \to H_2$ and $g_2 : H_2 \to H_3$, we have

$$F(g_2 \circ g_1) = F((g_{2,N} \circ g_{1,N}, g_{2,E} \circ g_{1,E})) = (g_{2,N} \circ g_{1,N}, g_{2,E} \circ g_{1,E}, (g_{2,A} \circ g_{1,A})) = F\,g_2 \circ F\,g_1.$$

Now we prove that F is full, faithful, and essentially surjective.

Full: Take two hypergraphs $H_1 = (N_1, E_1)$ and $H_2 = (N_2, E_2)$, so $F\,H_1 = (N_1 \sqcup E_1, A_1)$ and $F\,H_2 = (N_2 \sqcup E_2, A_2)$.

Let $f = (f_1, f_2, f_A) : F\,H_1 \to F\,H_2$ be a morphism in **BiparGraph**. Define $g = (f_1, f_2) : H_1 \to H_2$. We need to verify that g is a morphism in **Hyper**.

For any $v \in N_1$ and $e \in E_1$ with $v \in e$, we have $(v,e) \in A_1$. Since f is a bipartite graph morphism, $(f_1(v), f_2(e)) \in A_2$, which means $f_1(v) \in f_2(e)$. Thus g preserves incidence and is a hypergraph morphism with $F\,g = f$.

Faithful: Consider two hypergraph morphisms $g_1, g_2 : H_1 \to H_2$. Suppose $F\,g_1 = F\,g_2$. Then:

$$F\,g_1 = (g_{1,N}, g_{1,E}, g_{1,A}) = (g_{2,N}, g_{2,E}, g_{2,A}) = F\,g_2$$

This implies $g_{1,N} = g_{2,N}$ and $g_{1,E} = g_{2,E}$, hence $g_1 = g_2$.

Dense: Given a bipartite graph $G = (V_1 \sqcup V_2, A)$, define the hypergraph $H = (N, E)$ where:

- $N = V_1$
- $E = V_2$, and for each $e \in V_2$, define the corresponding hyperedge as the set $\{v \in V_1 \mid (v,e) \in A\}$

Then $F\,H = (V_1 \sqcup V_2, \{(v,e) \mid v \in V_1, e \in V_2, v \in e\}) = (V_1 \sqcup V_2, A) = G$.

Thus $G = F\,H$.

Since F is full, faithful, and dense, the categories **Hyper** and **BiparGraph** are equivalent. □

Appendix B: Frequency tuning for global synchronization

1. Relation to prior works

The problem of global frequency synchronization in Kuramoto oscillator networks concerns the conditions under which all oscillators eventually converge to a common frequency, despite differences in their natural frequencies and complex interaction structures. This problem has attracted broad theoretical and applied interest due to its relevance in diverse systems from neuroscience to power grids. Recent works have extended classical Kuramoto models to incorporate higher-order interactions beyond pairwise couplings, revealing richer dynamics and novel synchronization phenomena. Notably, Dutta et al. have advanced the theoretical understanding of perfect synchronization in complex networks with higher-order interactions and phase frustrations [31, 47, 48], while Muolo et al. [39] demonstrated cases where higher-order interactions can significantly enhance synchronization robustness and efficiency.

In this section, we adopt a constructive approach to global frequency synchronization in Kuramoto models with both 2-body and 3-body interactions governed by frustration parameters. Rather than attempting to eliminate frustration through topological modifications or coupling adjustments, our method exploits the hypergraph structure and assigns natural frequencies to individual oscillators in such a way that global frequency synchronization becomes achievable despite the presence of frustration. Our approach is closely related to a line of research where synchronization is achieved not only through network topology or coupling strength, but also by shaping the intrinsic frequencies or phase-lags of the oscillators. A recent example is the work of Ocampo-Espíndola et al. [49], who demonstrated that a structured detuning of natural frequencies can induce global frequency synchronization. While their mechanism relies

on introducing carefully designed frequency heterogeneity, our strategy can be seen as its complementary counterpart: we fix frustration parameters $(\alpha^{(2)}, \alpha^{(3)})$ and then solve for the natural frequencies that make global synchronization compatible with the hypergraph structure. Earlier studies, such as Brede et al. [30], explored how phase-lags in the Kuramoto-Sakaguchi model on graphs can achieve perfect synchronization. We extend these findings to higher-order contexts, inverting their approach by fixing frustration parameters and choosing a suitable frequency configuration to balance multi-body frustration. It is worth noting that our frequency assignment formula bears a similarity to the approach developed by Dutta et al. [47] for perfect synchronization in complex networks with higher-order interactions. Both methods prescribe natural frequencies as degree-weighted corrections involving frustration parameters. However, there are important structural differences beyond the conceptual frameworks. Dutta et al. work within the Kuramoto-Sakaguchi model framework on simplicial complexes, and employs a different formulation for 3-body interactions of the form $\sin(2\theta_i - \theta_j - \theta_k - \beta)$ rather than $\sin(\theta_j + \theta_k - 2\theta_i - \beta)$, and their approach focuses on achieving perfect synchronization (both phase and frequency) at targeted coupling strengths for arbitrary initial conditions. However, this common result suggests that degree-based frequency corrections represent a principle for controlling synchronization in higher-order Kuramoto models, regardless of the specific implementation strategy or interaction formulation.

2. Derivation of natural frequencies

Rather than analyzing the conditions under which an arbitrary system evolves toward synchronization, we adopt a constructive approach: we determine the natural frequencies ω_i for all nodes $i \in N$ that ensure the system starts in a frequency-synchronized state and remains there by design. The key insight is to recognize that frequency synchronization $\dot{\theta}_i = \Omega$ for all i represents a fixed point of the dynamics in velocity space. By selecting natural frequencies based on system parameters so that this condition is initially satisfied and preserved by the dynamics, we achieve perfect frequency synchronization right from the start.

Identical initial conditions To derive the required natural frequencies, we impose the synchronization condition $\dot{\theta}_i = \Omega$ and consider the case where all oscillators start from identical initial phases $\theta_i(0) = \theta_0$. Under these conditions, all phase differences are initially zero, which simplifies the interaction terms significantly. In detail, consider the Equation (1):

$$\dot{\theta}_i = \omega_i + \sigma_2 \sum_{e \in \mathcal{E}^{(2)}} [I^{(2)}]_{i,e} \sin\Big(\sum_{j \in e \setminus \{i\}} \theta_j - \theta_i - \alpha^{(2)} \Big) + \sigma_3 \sum_{e \in \mathcal{E}^{(3)}} [I^{(3)}]_{i,e} \sin\Big(\sum_{j \in e \setminus \{i\}} \theta_j - 2\theta_i - \alpha^{(3)} \Big). \tag{B1}$$

At $t = 0$, when $\theta_j(0) - \theta_i(0) = 0$ and $\theta_j(0) + \theta_k(0) - 2\theta_i(0) = 0$, the dynamical Equation (B1) becomes:

$$\Omega = \omega_i - \sigma_2 k_i^{(2)} \sin\left(\alpha^{(2)}\right) - \sigma_3 k_i^{(3)} \sin\left(\alpha^{(3)}\right)$$

where $k_i^{(2)}$ and $k_i^{(3)}$ represent the degrees of node i with respect to 2-body and 3-body interactions, respectively. Solving for the natural frequencies yields:

$$\omega_i = \Omega + \sigma_2 k_i^{(2)} \sin\left(\alpha^{(2)}\right) + \sigma_3 k_i^{(3)} \sin\left(\alpha^{(3)}\right) \tag{B2}$$

By starting all oscillators with identical phases and assigning natural frequencies according to Equation (B2), we ensure that all oscillators begin with the same instantaneous frequency Ω. Furthermore, since frequency synchronization is a fixed point of the dynamics, the system maintains this synchronized state indefinitely. At $t = 0$, all phases are equal, so phase differences are zero and all instantaneous frequencies are equal to Ω by design. Since for all nodes $i, j \in N$ we have $\dot{\theta}_i = \dot{\theta}_j = \Omega$, phase differences remain zero: $\dot{\theta}_{ij} = 0$. With zero phase differences maintained, the interaction terms remain constant. Therefore, $\dot{\theta}_i = \Omega$ is preserved for all time and nodes. Further, with the choice of identical initial conditions for all nodes, we have not only a global synchronization in frequency, but also in phase. As all the nodes start from the same condition and rotate with the same frequencies. Each oscillator's natural frequency is adjusted to compensate for the frequency shifts induced by its local network environment. Nodes with higher degrees in the interaction hypergraph require correspondingly larger frequency corrections to maintain global synchronization. Observe that ω_i depends only on the local incidence structure of node i. As a consequence, all nodes sharing the same multi-order degree profile necessarily receive the same intrinsic frequency and thus remain perfectly synchronized. In particular, nodes belonging to the same fibre of the hypergraph will evolve identically.

Random initial conditions Now we want to investigate the case in which the initial conditions are taken randomly from a uniform distribution in an interval $[0, \Delta]$. What happens when Δ changes?

The goal is to find an approximate bound for the initial condition spread to respect a tolerance condition for the deviation of each node's frequency from the chosen common frequency Ω. Initial phases are uniformly sampled from

$(0, \Delta)$: $\theta_i(0) \sim \mathcal{U}(0, \Delta)$ for $i = 1, \ldots, N$. This means: $\delta_i = \theta_i(0) \in [0, \Delta]$. For approximate frequency synchronization, we need:

$$|\dot{\theta}_i(0) - \Omega| \leq \tau \quad \forall i \in N,$$

where τ is the tolerance we fix. We substitute this expression at $t = 0$ in Equation (B1) and we use the trigonometric equation for the sine of the sum of angles:

$$\begin{aligned}
&\sin(\delta_j - \delta_i - \alpha^{(2)}) = \sin(\delta_j - \delta_i)\cos(\alpha^{(2)}) - \cos(\delta_j - \delta_i)\sin(\alpha^{(2)}),\\
&\sin(\delta_h + \delta_k - 2\delta_i - \alpha^{(3)}) = \sin(\delta_h + \delta_k - 2\delta_i)\cos(\alpha^{(3)}) - \cos(\delta_h + \delta_k - 2\delta_i)\sin(\alpha^{(3)}).
\end{aligned}$$

For small perturbations, since $|\delta_j - \delta_i|$ is small, we can use: $\sin(\delta_j - \delta_i) \approx \delta_j - \delta_i$ and $\cos(\delta_j - \delta_i) \approx 1$. Therefore:

$$\begin{aligned}
&\sin(\delta_j - \delta_i - \alpha^{(2)}) \approx (\delta_j - \delta_i)\cos(\alpha^{(2)}) - \sin(\alpha^{(2)}),\\
&\sin(\delta_h + \delta_k - 2\delta_i - \alpha^{(3)}) \approx (\delta_h + \delta_k - 2\delta_i)\cos(\alpha^{(3)}) - \sin(\alpha^{(3)}).
\end{aligned}$$

Putting all together, we obtain:

$$|\dot{\theta}_i(0) - \Omega| \approx \left| \sigma_2 \cos(\alpha^{(2)}) \sum_{e=\{i,j\}\in\mathcal{E}^{(2)}} (\delta_j - \delta_i) + \sigma_3 \cos(\alpha^{(3)}) \sum_{e=\{i,h,k\}\in\mathcal{E}^{(3)}} (\delta_h + \delta_k - 2\delta_i) \right|.$$

Since initial conditions are drawn from $[0, \Delta]$, the maximum possible difference $|\delta_j - \delta_i|$ is Δ, and for the 3-body term $|\delta_h + \delta_k - 2\delta_i|$ is at most 2Δ. The worst-case deviation for node i is thus bounded by:

$$|\dot{\theta}_i(0) - \Omega| \leq |\sigma_2 \cos(\alpha^{(2)})| k_i^{(2)} \Delta + 2|\sigma_3 \cos(\alpha^{(3)})| k_i^{(3)} \Delta.$$

For the tolerance condition to hold for all nodes, we need:

$$\Delta \left[|\sigma_2 \cos(\alpha^{(2)})| k_i^{(2)} + 2|\sigma_3 \cos(\alpha^{(3)})| k_i^{(3)} \right] \leq \tau \quad \forall i.$$

Therefore:

$$\Delta \leq \frac{\tau}{|\sigma_2 \cos(\alpha^{(2)})| k_i^{(2)} + 2|\sigma_3 \cos(\alpha^{(3)})| k_i^{(3)}}.$$

Since this must hold for all nodes, we need:

$$\Delta \leq \min_{i\in\{1,\ldots,N\}} \frac{\tau}{|\sigma_2 \cos(\alpha^{(2)})| k_i^{(2)} + 2|\sigma_3 \cos(\alpha^{(3)})| k_i^{(3)}}.$$

To obtain a simplified form, define $\kappa_i := |\sigma_2 \cos(\alpha^{(2)})| k_i^{(2)} + 2|\sigma_3 \cos(\alpha^{(3)})| k_i^{(3)}$. Then

$$\Delta_{\max} = \frac{\tau}{\max_i \kappa_i}.$$

For the linearization to remain valid, we also require $\Delta \ll 0.5$ to ensure $\max_{i,j,h,k}\{|\delta_j - \delta_i|, |\delta_h + \delta_k - 2\delta_i|\} \ll 1$. Hence:

$$\Delta_{\max} = \min\left\{ \frac{\tau}{\max_i \kappa_i}, 0.1 \right\}. \tag{B3}$$

Remark B.1. The bound $\Delta_{\max}$ depends on several factors:

- Tolerance τ: stricter tolerance requires smaller Δ.
- Coupling strengths σ_2, σ_3: stronger coupling requires smaller Δ.
- Frustration parameters via $|\cos(\alpha^{(2)})|, |\cos(\alpha^{(3)})|$: values closer to $\pi/2$ allow larger Δ.
- Network topology: the most highly connected node determines the constraint, with 3-body interactions being twice as constraining as 2-body interactions for the same degree.

Stability analysis The bound derived above ensures frequency deviations remain small at $t = 0$. For the bound to remain valid for all $t > 0$, the frequency-synchronized manifold must be linearly stable. The frustration parameters $\alpha^{(k)}$ play two distinct roles: frequency balancing through $\sin(\alpha^{(k)})$ terms, which determine the required natural frequency adjustments in Equation (B2), and stability control through $\cos(\alpha^{(k)})$ terms, which govern the evolution of perturbations around the synchronized state. When the system is frequency synchronized, each node evolves as $\theta_i(t) = \Omega t + \theta_0$. Let $\phi_i(t) = \theta_i(t) - (\Omega t + \theta_0)$ be the perturbation of node i from the synchronized state. The linearized dynamics around the synchronized state are:

$$\dot{\phi}_i = -\sigma_2 \cos(\alpha^{(2)}) \sum_{e=\{i,j\}\in\mathcal{E}^{(2)}} (\phi_j - \phi_i) - \sigma_3 \cos(\alpha^{(3)}) \sum_{e=\{i,h,k\}\in\mathcal{E}^{(3)}} (\phi_h + \phi_k - 2\phi_i).$$

This system can be written as $\dot{\phi} = -L\phi$ where L is an effective Laplacian matrix combining the 2-body and 3-body interaction topologies, weighted by $\sigma_2 \cos(\alpha^{(2)})$ and $\sigma_3 \cos(\alpha^{(3)})$ respectively. The synchronized state is linearly stable when all non-zero eigenvalues of L are positive, which requires both effective coupling coefficients to be positive:

$$\cos(\alpha^{(2)}) > 0 \quad \text{and} \quad \cos(\alpha^{(3)}) > 0.$$

This corresponds to the condition $\alpha^{(k)} \in (0, \pi/2)$ for $k \in \{2, 3\}$.

Although our analysis of global frequency synchronisation no longer explicitly depends on the fibre structure, it is quite remarkable that, by selecting appropriate initial conditions fibre-coherent, it is still possible to identify the underlying fibres, albeit only through subtle phase differences. A concrete example of this phenomenon is provided in Figure 15, where numerical simulations illustrate how appropriately chosen initial conditions reveal the underlying fibre organization despite overall frequency locking.

3. Simulations

To investigate the synchronization properties of the higher-order Kuramoto model, we performed numerical simulations tracking the evolution of individual node frequencies and their deviations from the network average. We create a connected hypergraph, and we choose the parameter set $(\sigma_2, \sigma_3, \alpha^{(2)}, \alpha^{(3)})$. We also set the desired common frequency Ω. Then, the natural frequencies are assigned according to Equation (B2), ensuring that each oscillator's intrinsic frequency compensates for the higher-order coupling effects it experiences based on its degrees. When all initial phases are identical, the system exhibits perfect global synchronization in both phase and frequency. This behavior is illustrated in an example with Figure 12, where all oscillators converge rapidly and collectively to the target common frequency Ω, with frequency dispersion across the hypergraph suppressed essentially from the outset. Furthermore, the global order parameter reaches 1, indicating global phase synchronization.

To probe robustness, we then consider random initial conditions uniformly sampled from $[0, \Delta]$. The resulting dynamics, shown in Figure 13, display the average deviation from Ω as a function of time for different choices of Δ. The dashed red line marks the admissible tolerance τ, while $\Delta_{\max}$ denotes the theoretical upper bound predicted by our analysis. We find that synchronization persists well beyond this bound: even for $\Delta \geq \Delta_{\max}$, the deviation remains below the tolerance. Thus, $\Delta_{\max}$ is a conservative estimate.

Finally, to show the influence of the frustration parameters on the stability of the result for $t > 0$, in Figure 14 we plot the average temporal evolution of the logarithmic frequency deviations from the target $\Omega = 2$ over 20 repetitions, changing the initial conditions randomly in $[0, \Delta_{\max}]$ for different frustration angles $\alpha = \alpha^{(2)} = \alpha^{(3)}$. The results show a separation between stable and unstable regimes dictated by the frustration parameters. For $\alpha^{(k)} < \pi/2$, the trajectories exhibit an exponential decay of frequency deviations, confirming the predicted stability condition $\cos(\alpha^{(k)}) > 0$. In contrast, angles beyond this limit fail to maintain only bounded oscillations around the desired frequency. While global frequency synchronization typically eliminates the relevance of fibre structure in the asymptotic dynamics, it is interesting to observe that by choosing ad hoc initial conditions, fibres can still be distinguished through small but persistent phase differences. Indeed, the initial conditions can be randomly distributed across fibres within the theoretical bound $[0, \Delta_{\max}]$. Then, we assign the same initial condition to the nodes in each fibre. Figure 15 illustrates the synchronization dynamics in a fibre-coherent network where the initial conditions are chosen in this way. The small size of the differences across different fibres is mainly because $\Delta_{\max}$ is small (≤ 0.1) and the number of fibres is of the same order as $|N|$. The key finding is that while nodes within individual fibres achieve perfect phase synchronization due to identical initial conditions (by construction) and natural frequencies (determined by their shared degree sequences), inter-fibre phase differences persist even after global frequency synchronization is established. The exponential decay of both minimum and maximum phase differences demonstrates the system's convergence toward a synchronized state, yet the asymptotic behavior reveals that at the beginning, fibres maintain distinct phase offsets relative to each other. This phenomenon arises from the random initial condition assignment:

nodes within each fibre inherit identical initial phases and natural frequencies, ensuring intra-fibre coherence, but the random distribution of these initial conditions across different fibres creates lasting phase disparities between fibre populations.

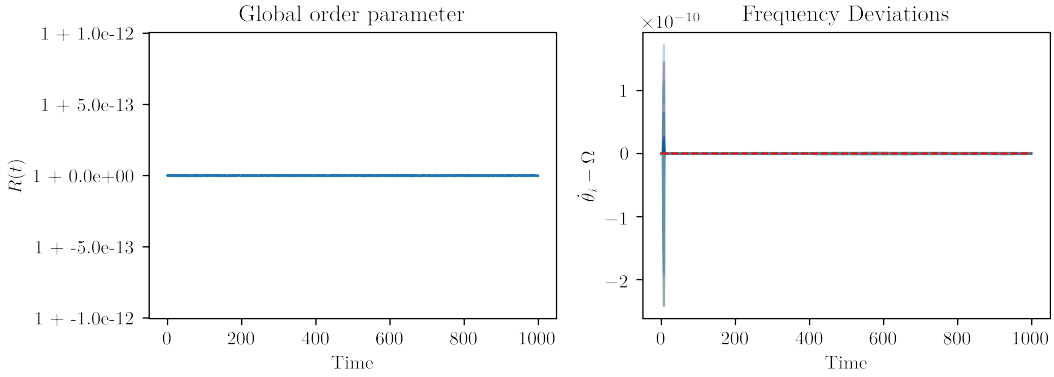

Figure 12: Starting from identical initial conditions, we simulate the higher-order Kuramoto model using the `dopri5` integrator over 1000 steps with $|N| = 188$, coupling strength $(\sigma_2, \sigma_3) = (0.6, 0.8)$, $\theta_0 = \pi/3$ and frustration parameters $(\alpha^{(2)}, \alpha^{(3)}) = (\pi/3, \pi/6)$. The desired common frequency to achieve is set to $\Omega = 2$. On the left, the global order parameter. On the right, the deviations $\dot{\theta} - \Omega$, illustrating the progressive reduction of frequency dispersion among nodes (in dashed red, the reference line of 0).

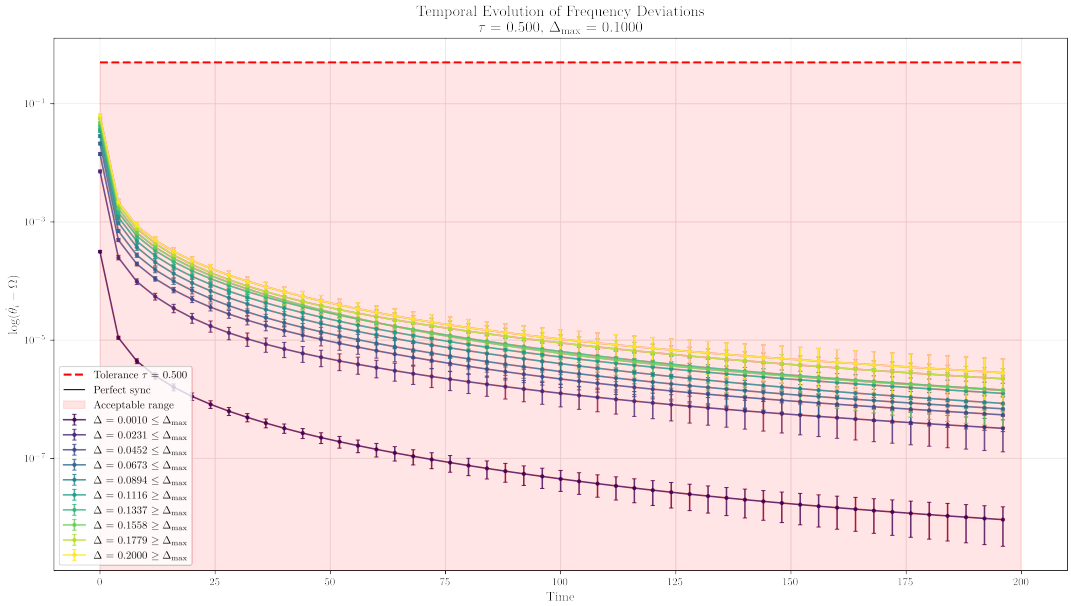

Figure 13: We simulate the higher-order Kuramoto model with random initial conditions uniformly drawn from $[0, \Delta]$, using the `dopri5` integrator over 1000 steps. The system has $|N| = 189$ nodes, coupling strengths $(\sigma_2, \sigma_3) = (0.6, 0.8)$, and frustration parameters $(\alpha^{(2)}, \alpha^{(3)}) = (\pi/3, \pi/3)$. The target common frequency is set to $\Omega = 2$. The plot shows the time evolution of the average deviation from Ω for different values of the upper bound Δ. The dashed red line marks the tolerance τ, while $\Delta_{\max}$ denotes the analytically predicted bound for these parameters (Equation (B3)). Results show that the theoretical bound is sufficient but not necessary: even when $\Delta \geq \Delta_{\max}$, the deviation stays below the tolerance, indicating that the condition is conservative.

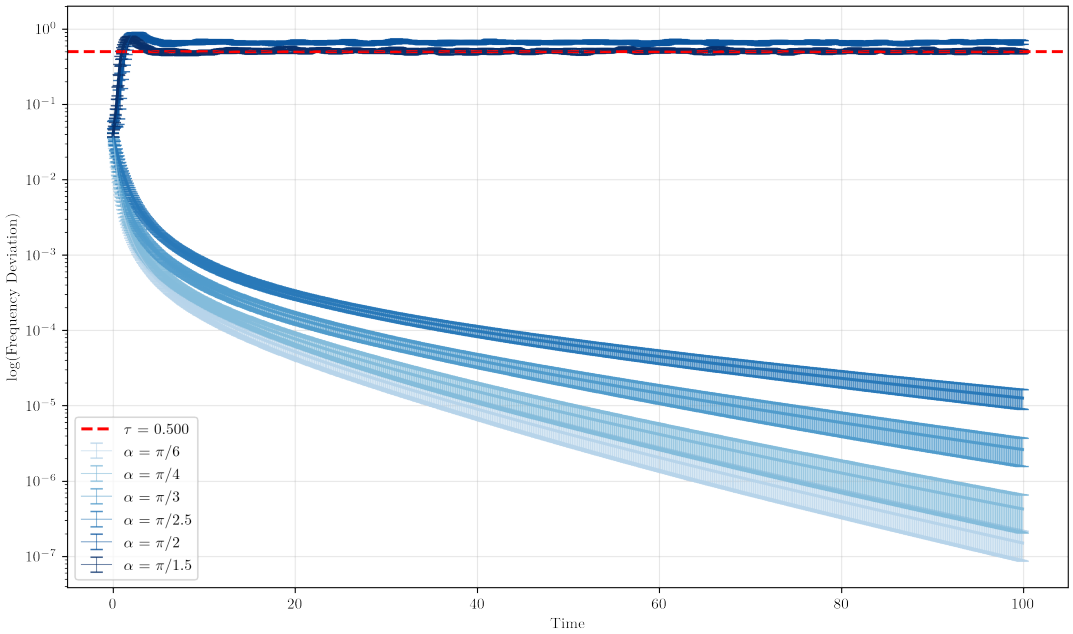

Figure 14: Temporal evolution of the logarithmic frequency deviations from the target $\Omega = 2$ for different frustration angles $\alpha = \alpha^{(2)} = \alpha^{(3)}$ in a higher-order Kuramoto system ($|N| = 189, T_{\max} = 100$, integration step 0.1, $\sigma_2 = 0.6$, $\sigma_3 = 0.8, \tau = 0.5$). We repeat the simulation 20 times, changing the initial conditions taken randomly in the interval $[0, \Delta_{\max}]$, with $\Delta_{\max}$ computed as in Equation (B3). Hence, we report the average and the standard deviation at each time across the repetitions. The dashed red line indicates the tolerance $\tau = 0.5$. We can observe that for $\alpha > \pi/2$, the limitation of the deviation is no longer valid for t increasing.

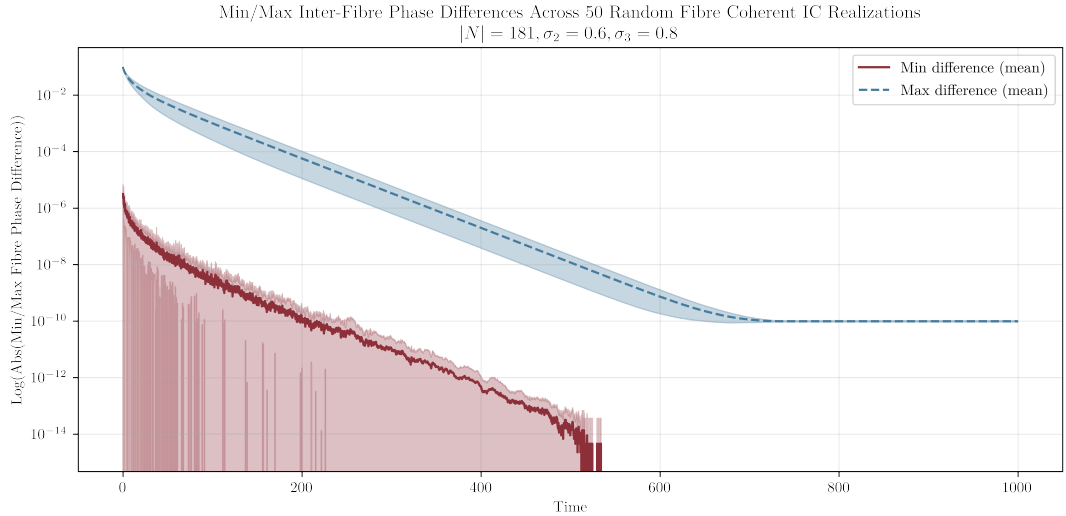

Figure 15: Temporal evolution of the avergae inter-fibre phase differences (minimum and maximum) across 50 random realizations in a higher-order Kuramoto system with fibre structure ($|N| = 181, T_{\max} = 100$, integration step 0.1, $\sigma_2 = 0.6$, $\sigma_3 = 0.8$). Initial conditions are randomly assigned to fibres within $[0, \Delta_{\max}]$, with all nodes in the same fibre sharing identical initial phases and natural frequencies. The solid red line shows the minimum phase differences between fibres, the dashed blue line represents the maximum differences, both averaged across realizations and with the confidence interval shadowed. Despite achieving global frequency synchronization, small persistent inter-fibre phase differences remain due to random initial condition assignment across fibres.